Описание распределений продуктов деления тяжелых ядер и их корреляция с множественностью нейтронов

H. Pasca, A. Andreev, G. Adamian, N. Antonenko

BLTP, JINR

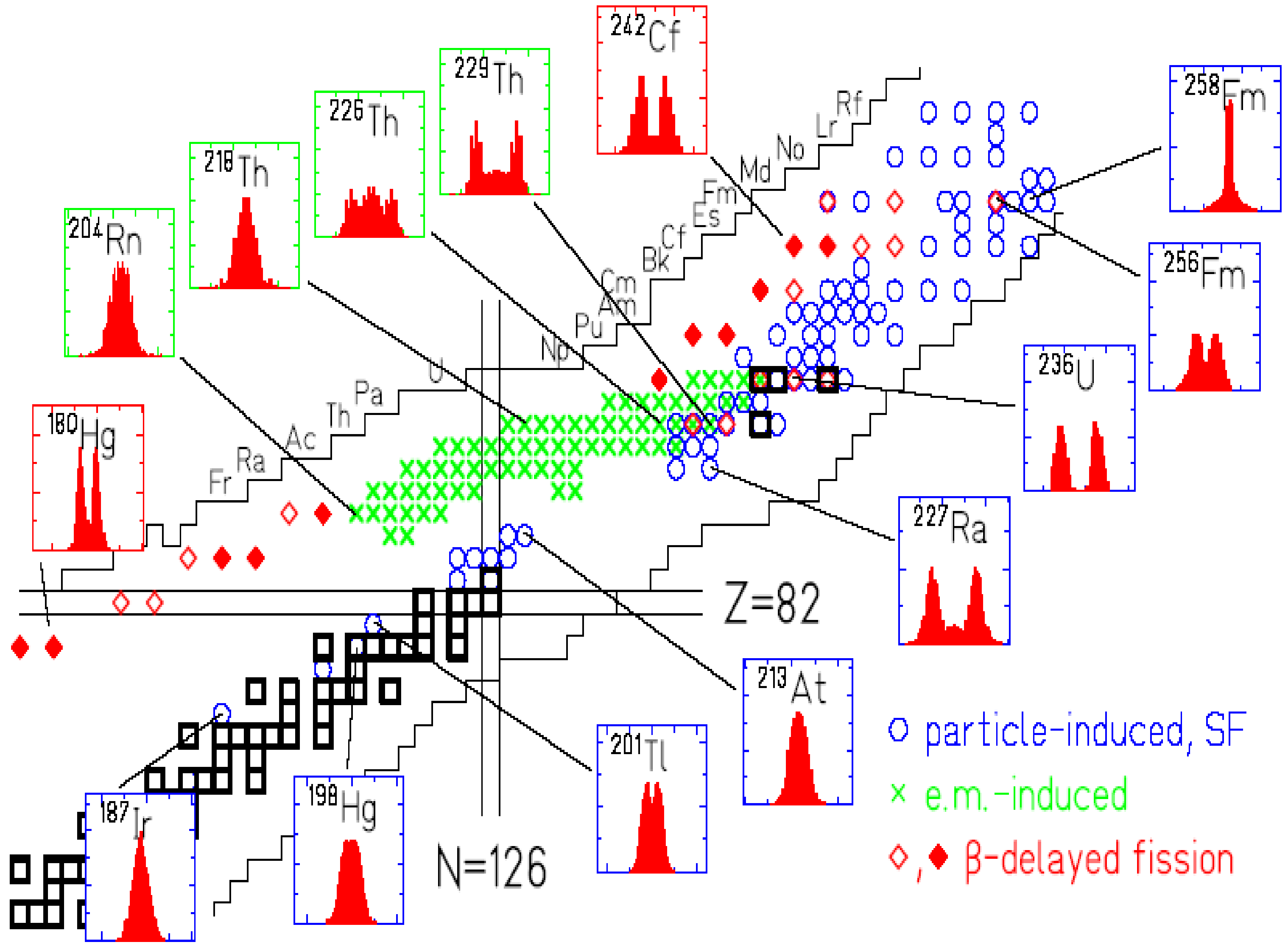

242Cf
229Th
226Th
218Th
204Rn
180Hg
258Fm
256Fm
236U
227Ra
213At
201Tl
198Hg
187Ir
Rf
Lr
No
Md
Fm
Es
Cf
Bk
Cm
Am
Pu
Np
U
Pa
Th
Ac
Ra
Fr
Z=82
N=126
particle-induced, SF
e.m.-induced
β-delayed fission

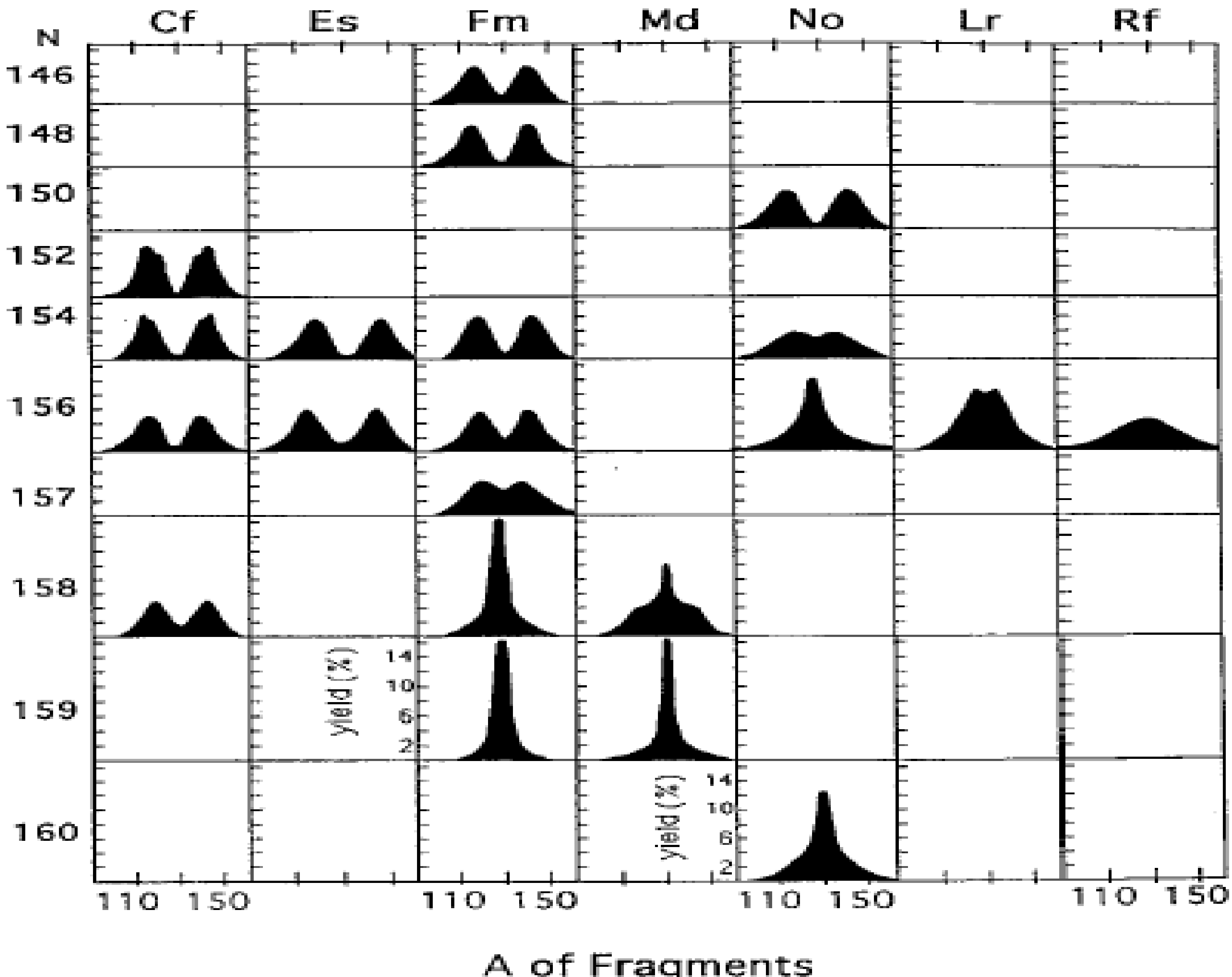
Cf
Es
Fm
Md
No
Lr
Rf
N
146
148
150
152
154
156
157
158
159
160
yield (%)
14
10
6
2
110
150
A of Fragments

<u>General opinion</u>:

The *competition between symmetric and asymmetric fission is related to shell effects* in deformed fissioning nucleus

U.Brosa, S.Grossmann, A.Muller, Phys.Rep.197(1990)167

Exper. data for high-energy (**60 MeV**) **neutron-induced fission of ^{238}U** shows the conservation of asymmetric mass distribution, even though shell effects are supposed to be damped.

I.V.Ryzhov et al. , PRC83(2011) 054603

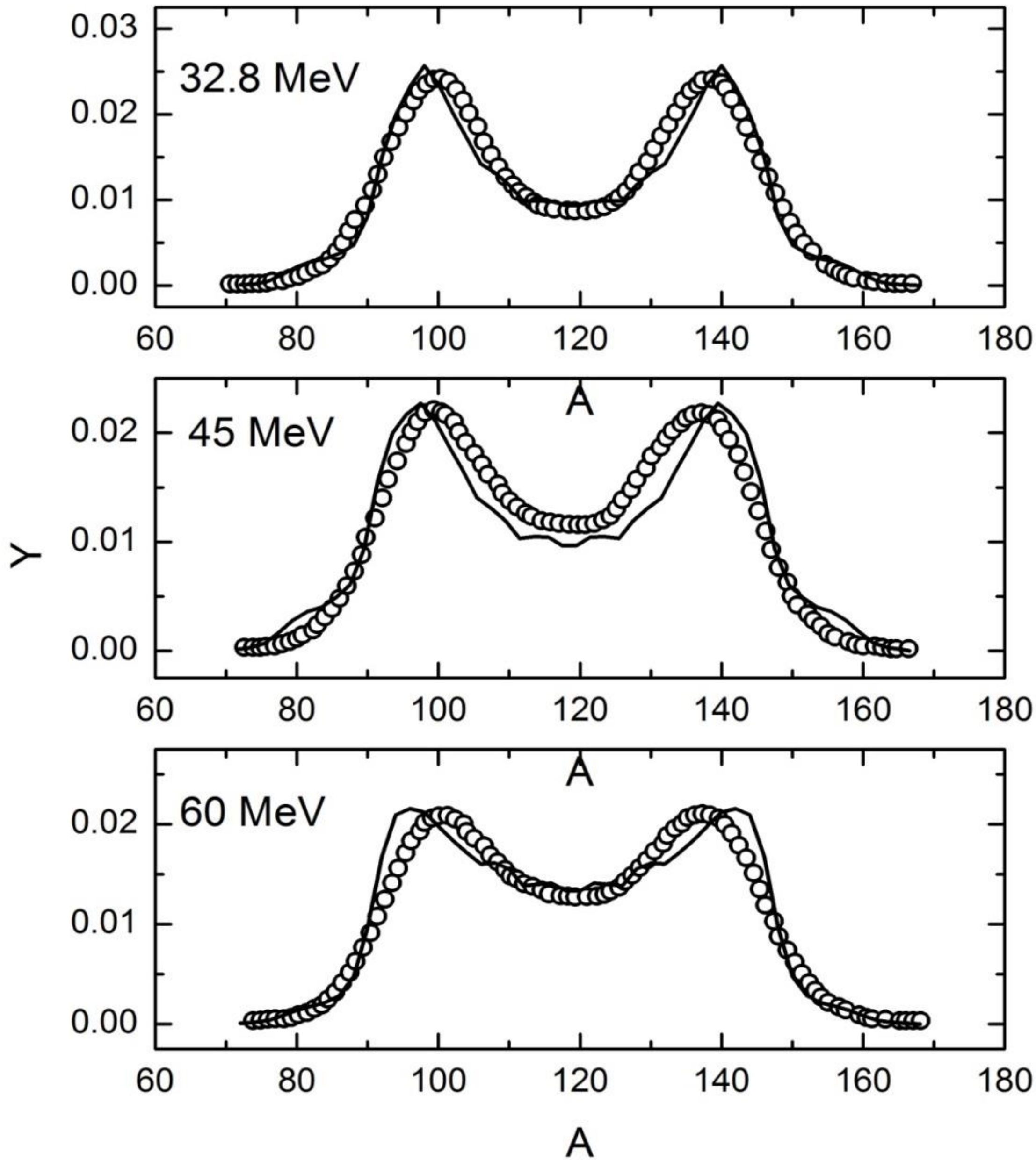

n + 238U

Exper. asymmetric mass yields result in fission of highly excited (~60 MeV) nuclei ^{232}Th, $^{237-240}$U, $^{239-242}$Np, $^{241-244}$Pu, produced in transfer reactions ^{18}O+^{232}Th,^{238}U,^{237}Np !

K.Hirose PRL **119** (17)222501; PLB **761** (16)125

^{232}Th(n,f) V.Simukhin NDS **119** (14) 331; J.King EPJA **53** (17) 238

Conservation of asymmetric mass distribution, even though shell effects are supposed to be damped

Statistical Scission-point Model
or
Cluster model of fission

- Scission-point model relies on assumption that the statistical equilibrium is established at scission where the observable characteristics of fission are formed.

- Scission system - two well-defined fission fragments in contact [dinuclear system=DNS].

Model

Coordinates Z_i, A_i, β_i (I = L, H), R completely describe the geometry of system

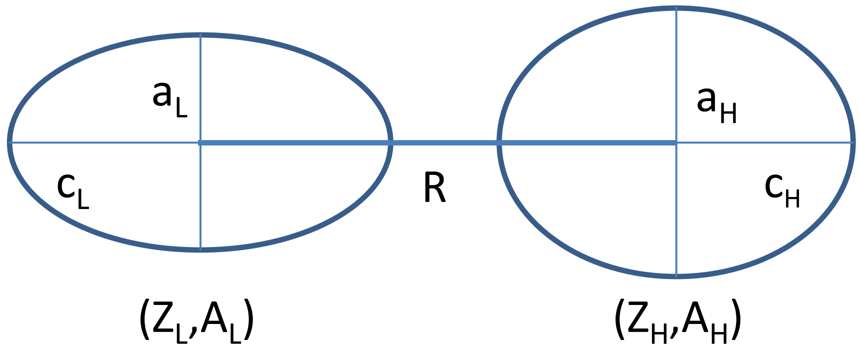

- ***Total Potential Energy*** *:*

$$
\begin{aligned}
U(A_i, Z_i, \beta_i, R) \\
&= U_L^{\mathrm{LD}}(A_L, Z_L, \beta_L) + \delta U_L^{\mathrm{shell}}(A_L, Z_L, \beta_L, E_H^*) \\
&\quad + U_H^{\mathrm{LD}}(A_H, Z_H, \beta_H) + \delta U_H^{\mathrm{shell}}(A_H, Z_H, \beta_H, E_H^*) \\
&\quad + V^C(A_i, Z_i, \beta_i, R) + V^N(A_i, Z_i, \beta_i, R)
\end{aligned}
$$

$V = V^C + V^N$ - ***interaction potential***

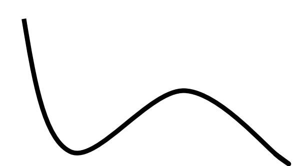

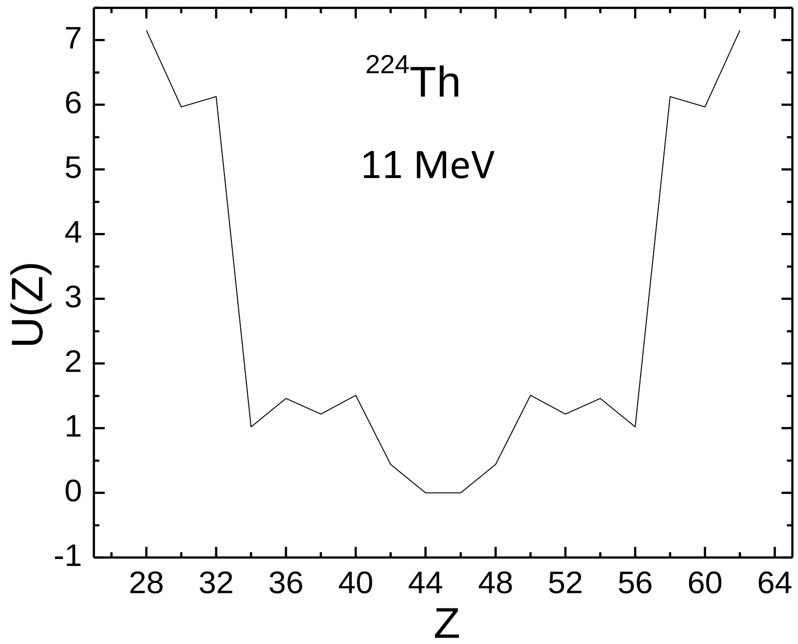

Minima in potential are result of interplay between liquid-drop, interaction, shell correction energies

1. **Liquid-drop energy** globally increases when mass number deviate from symmetry.

2. **Interaction energy** has the opposite behavior.

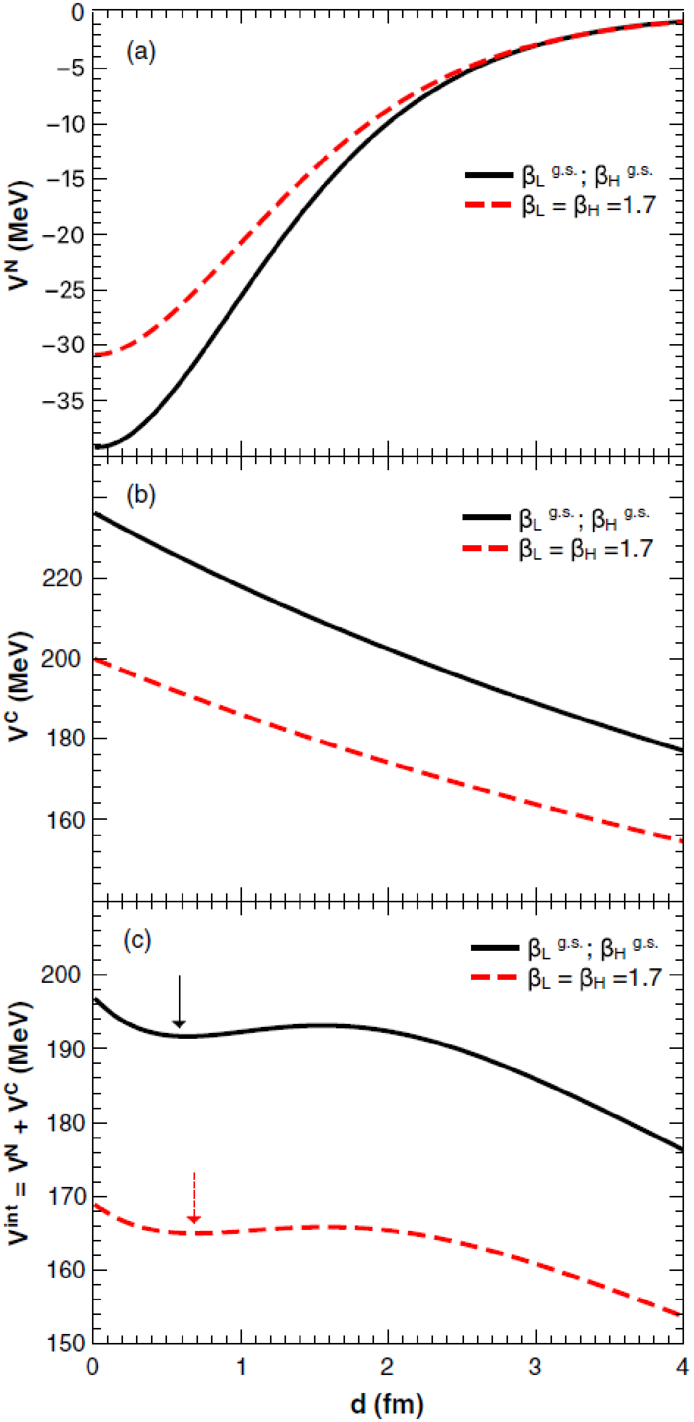

The calculated nuclear V^N and Coulomb V^C interaction potentials and their sum $V^{int} = V^N + V^C$ as a function of the distance d between the tips of the fragments for the fragmentation $^{222}Th \to {}^{110}Ru + {}^{112}Pd$. The position of the interaction potential pocket minimum is indicated by the arrow. The deformations $\beta_{L,H}$ of the DNS nuclei are indicated.

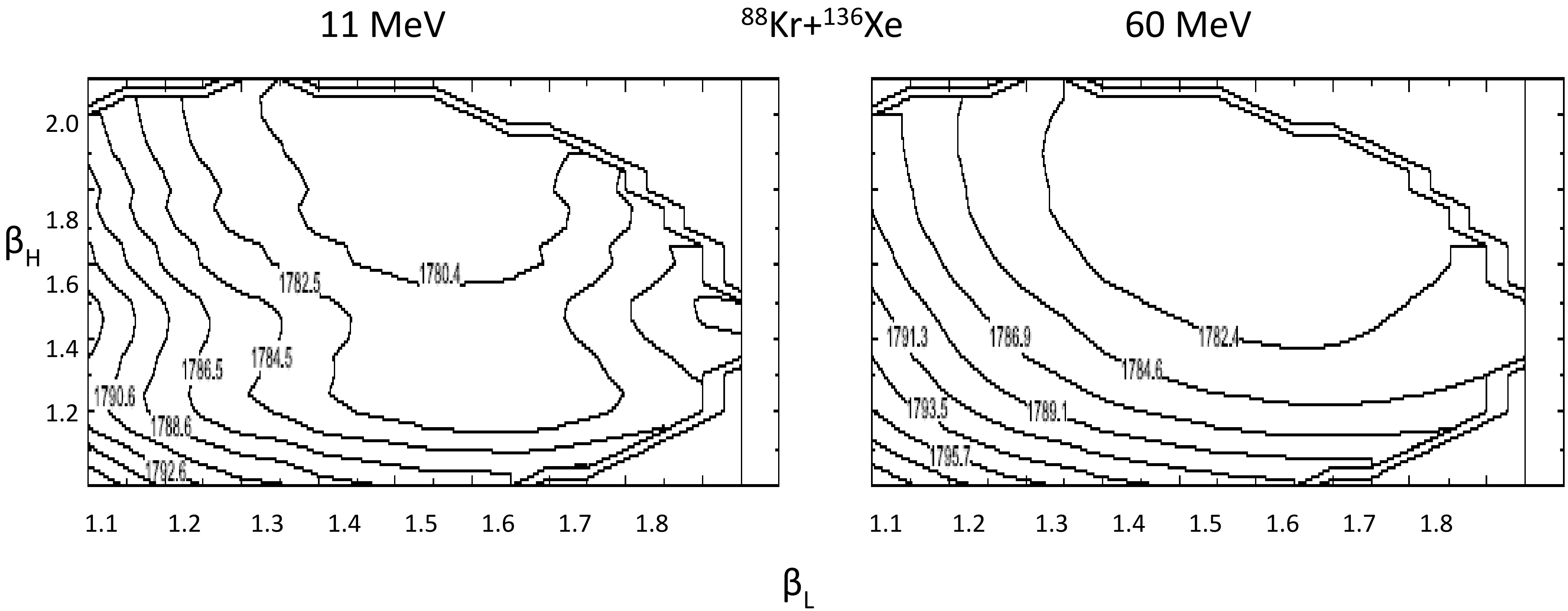

Minimum becomes wider, migrates to larger deformations with increasing excitation energy

Ratio of yields of fragments with different charge/mass is governed by difference in energy and width between their potential minima in PES (β_L, β_H).

If two minima are close in energy, higher yield stems from with wider-shallower minimum, lower yield emerges from abrupt-narrow minimum.

Model

Yields:

$$w(A_i, Z_i, \beta_i, E^*) = N_0 \exp\left[-\frac{U(A_i, Z_i, \beta_i, R_b)}{T}\right]$$

$$Y(A_i, Z_i, E^*) = \int d\beta_L d\beta_H w(A_i, Z_i, \beta_i, E^*)$$

$$Y(A_i, E^*) = \frac{\sum_{Z_i} Y(A_i, Z_i, E^*)}{\sum_{Z_i, A_i} Y(A_i, Z_i, E^*)},$$

$$Y(Z_i, E^*) = \frac{\sum_{A_i} Y(A_i, Z_i, E^*)}{\sum_{Z_i, A_i} Y(A_i, Z_i, E^*)}.$$

$$\mathrm{TKE}(A_i, Z_i, \beta_i) = V^C(A_i, Z_i, \beta_i, R_b) + V^N(A_i, Z_i, \beta_i, R_b),$$

$$\langle \mathrm{TKE} \rangle (Z_i) = \frac{\sum_{A_i} \int d\beta_L d\beta_H \mathrm{TKE}(A_i, Z_i, \beta_i) w(A_i, Z_i, \beta_i, E^*)}{\sum_{A_i} \int d\beta_L d\beta_H w(A_i, Z_i, \beta_i, E^*)}.$$

$$\langle n \rangle (Z_i) = \frac{\sum_{A_i} \int d\beta_L d\beta_H n(A_i, Z_i, \beta_i) w(A_i, Z_i, \beta_i, E^*)}{\sum_{A_i} \int d\beta_L d\beta_H w(A_i, Z_i, \beta_i, E^*)},$$

$$n(A_i, Z_i, \beta_i) = \sum_{i=L,H} \frac{E_i^*(A_i, Z_i, \beta_i) + E_i^{\mathrm{def}}(A_i, Z_i, \beta_i)}{S_i^n + 2T_i}.$$

The values of S_i^n are the average separation energies of the first two neutrons.

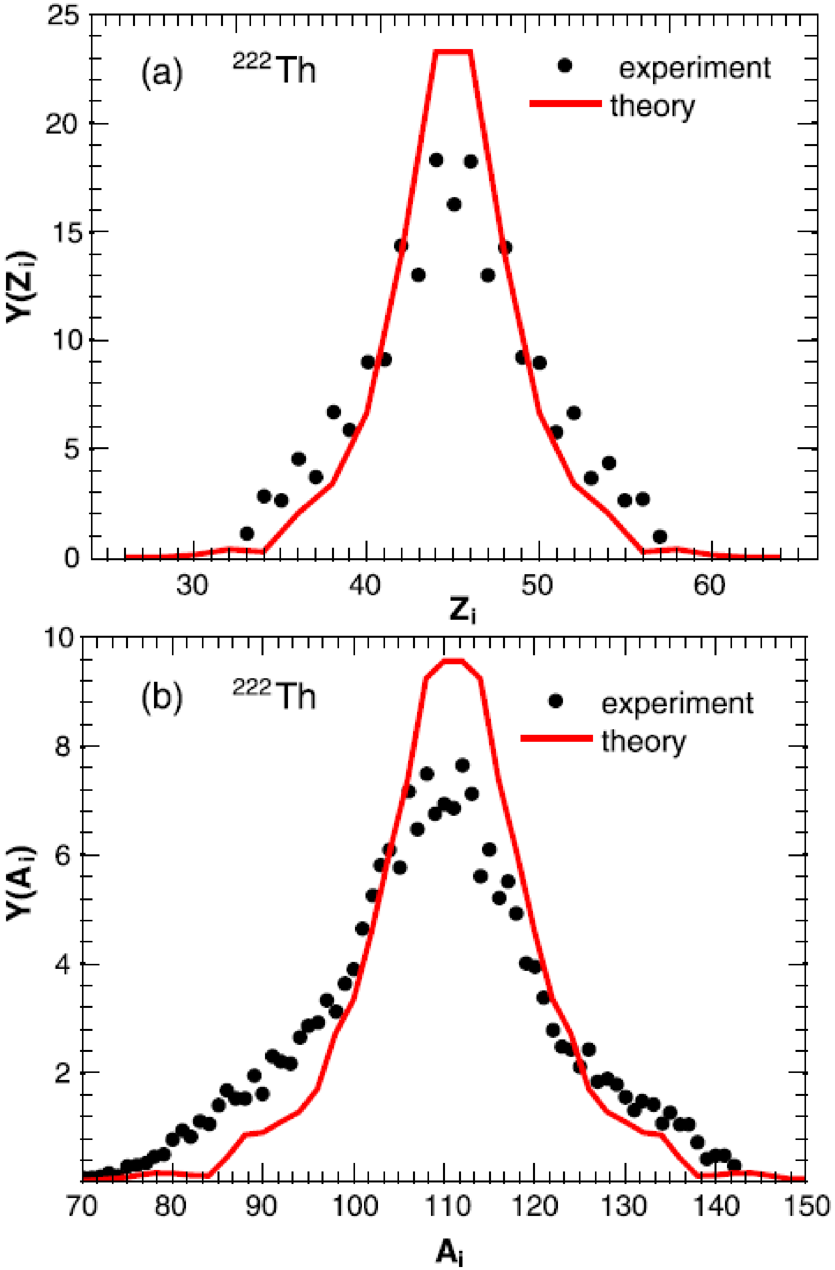

The calculated (lines) and experimental (symbols) [NPA **665**, 221 (2000); **693**, 169 (2001); PRL **124**, 202502 (2020)] charge (a) and mass (b) distributions of fission fragments for electromagnetic induced fission of ^{222}Th at 11 MeV excitation energy. The lines connect the calculated points for even-even fission fragments.

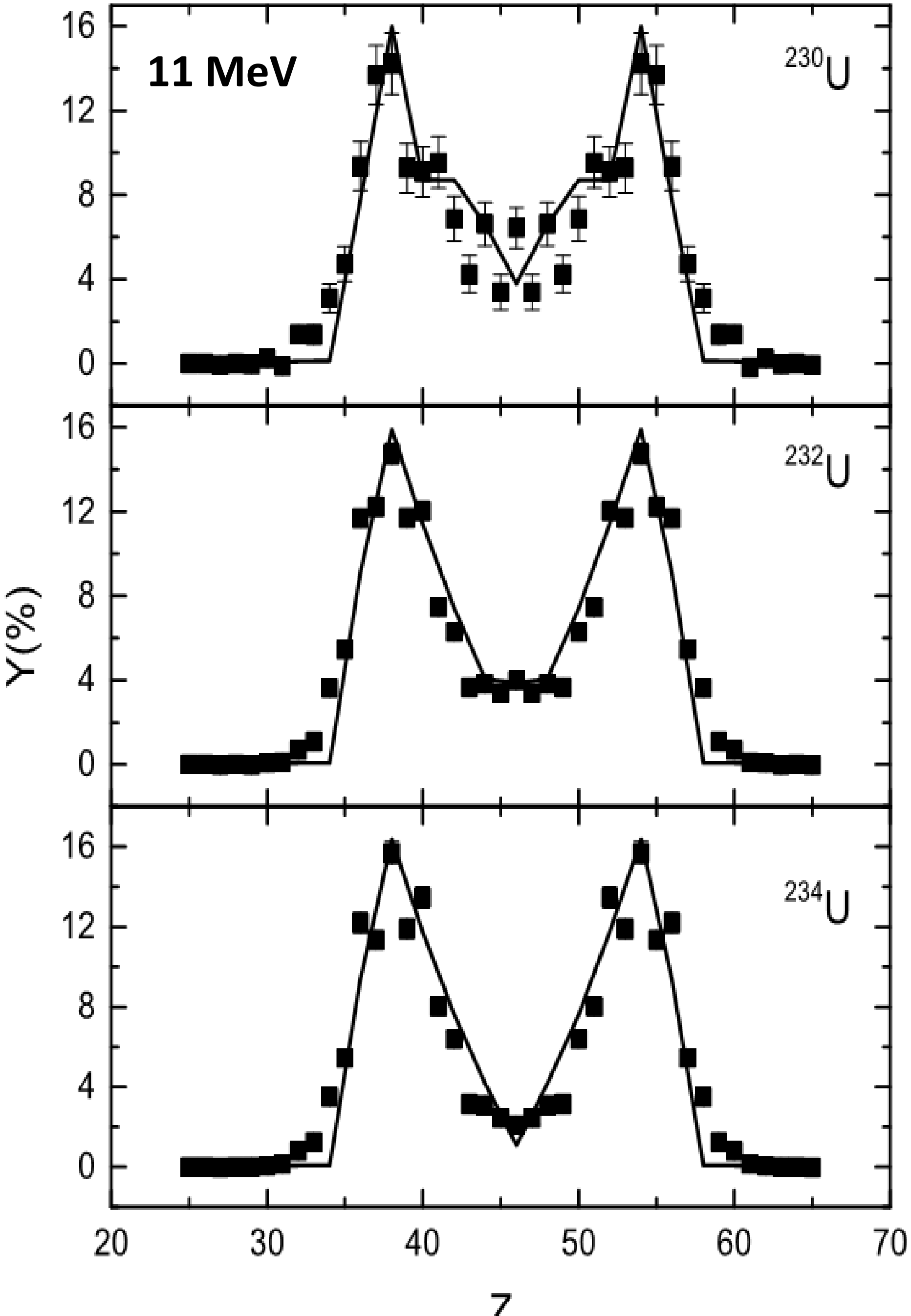

Calculated charge distributions for electromagnetic-induced fission of $^{230\text{-}234}U$ at exc. energy about 11 MeV

Exper. : K.-H.Schmidt *et al.*, NPA 665(2000)221.

Model is well suited for describing both asymmetric and symmetric fission distributions as well as transition between two.

High excitation energy of fissioning nucleus

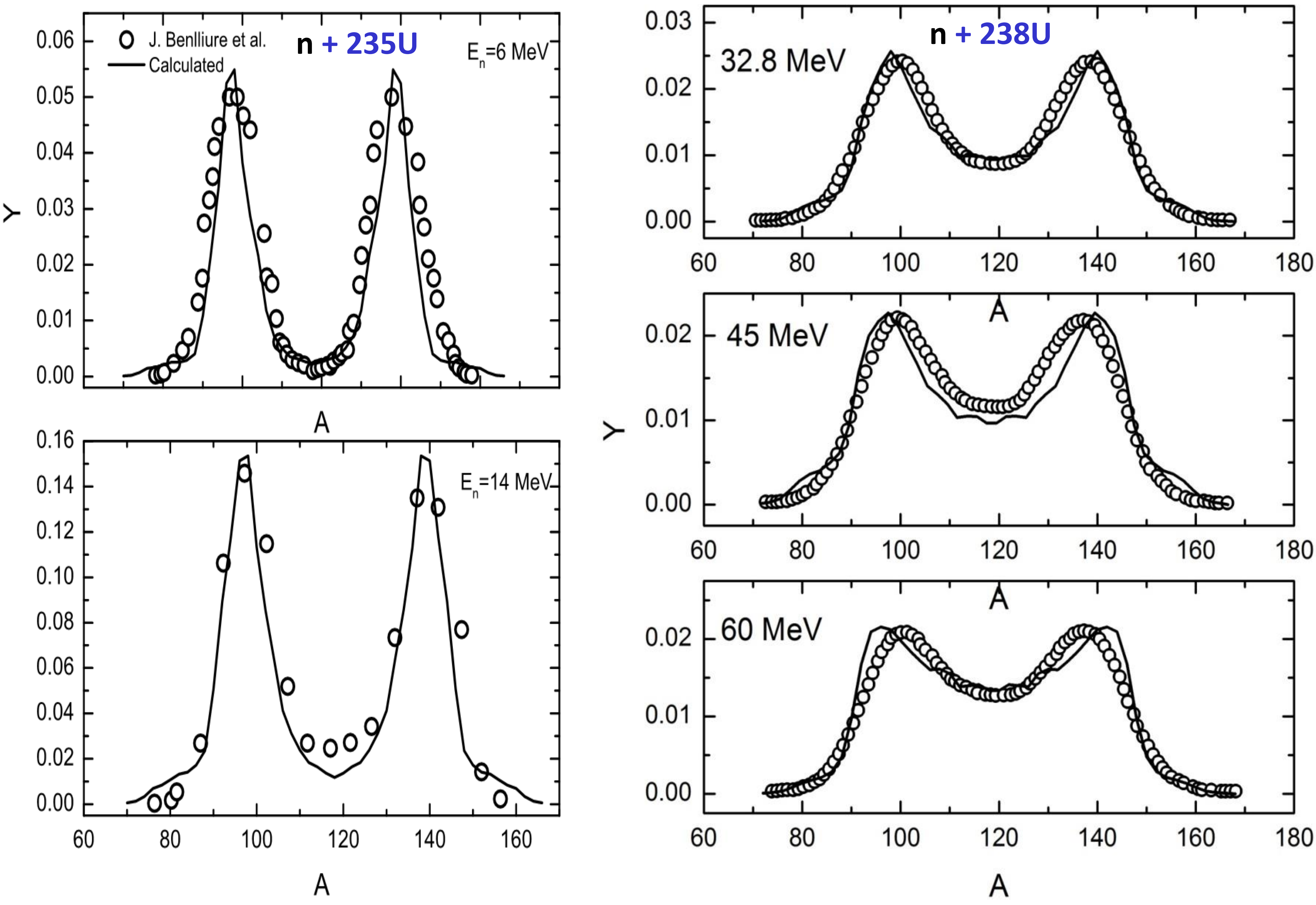

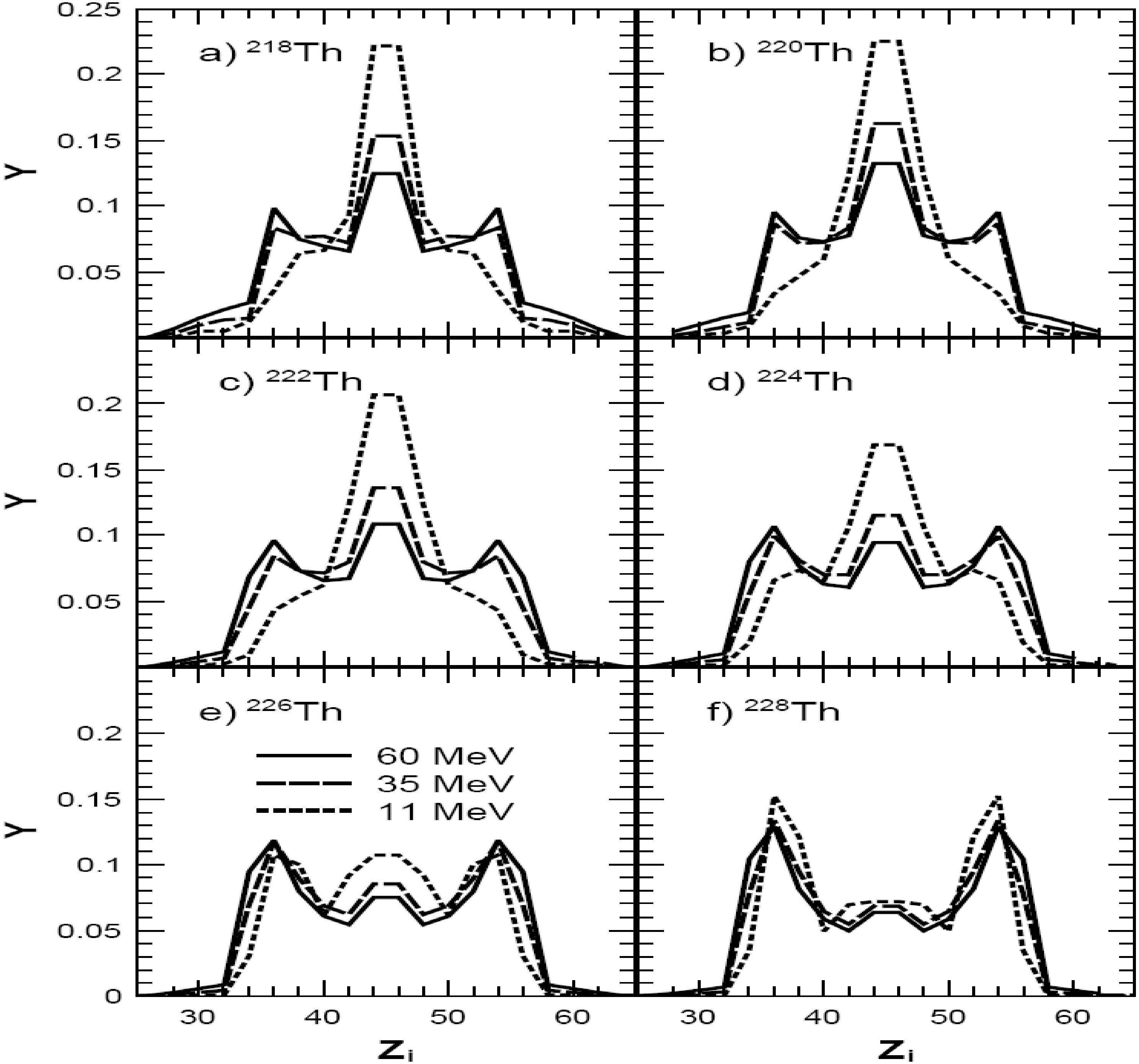

a) ^{218}Th
b) ^{220}Th
c) ^{222}Th
d) ^{224}Th
e) ^{226}Th
f) ^{228}Th
60 MeV
35 MeV
11 MeV
Y
Z_i
0
0.05
0.1
0.15
0.2
0.25
30
40
50
60

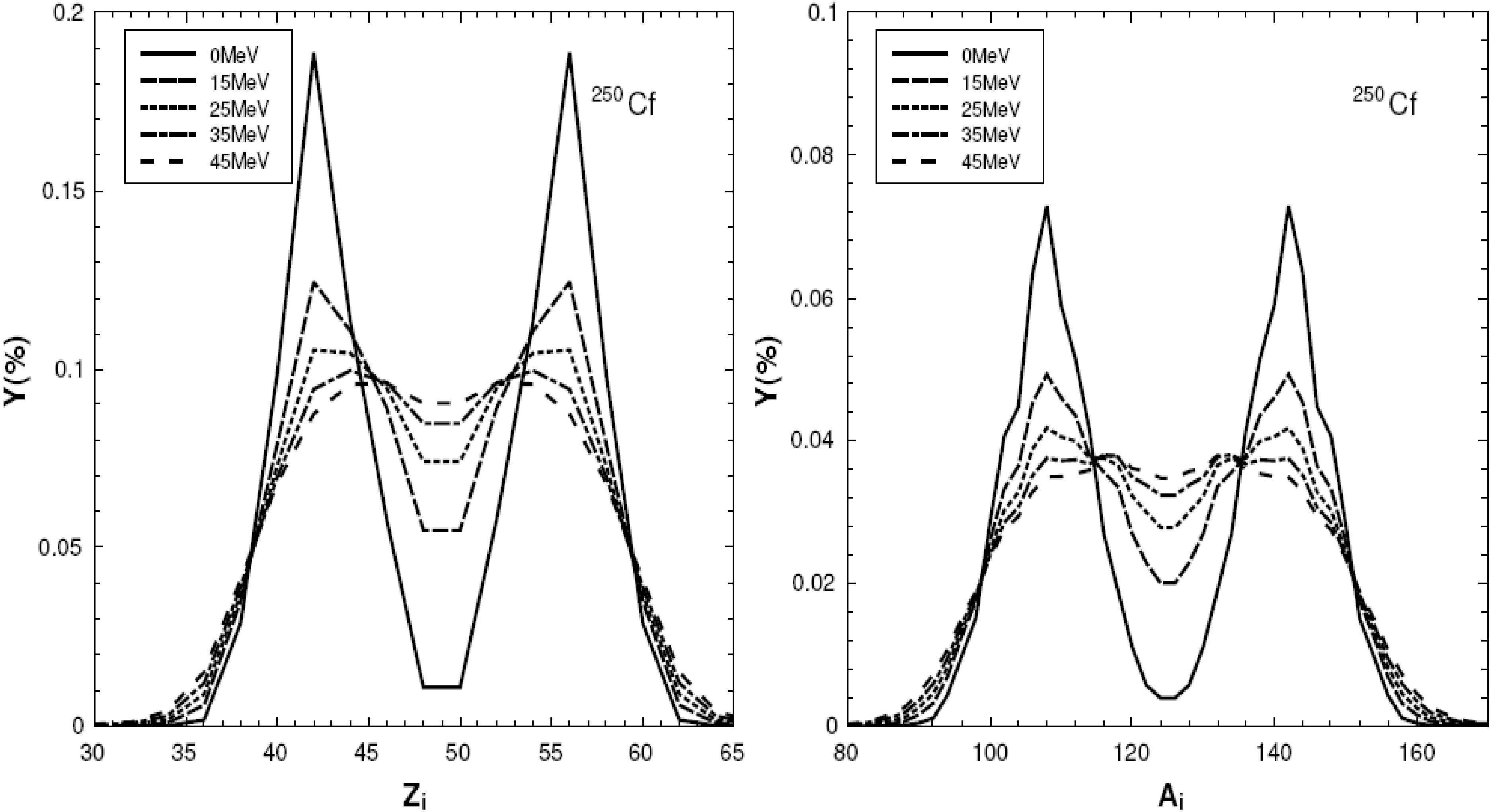

0MeV
15MeV
25MeV
35MeV
45MeV
^{250}Cf
Y(%)
Z_i
0MeV
15MeV
25MeV
35MeV
45MeV
^{250}Cf
Y(%)
A_i

Fission of heavy actinides

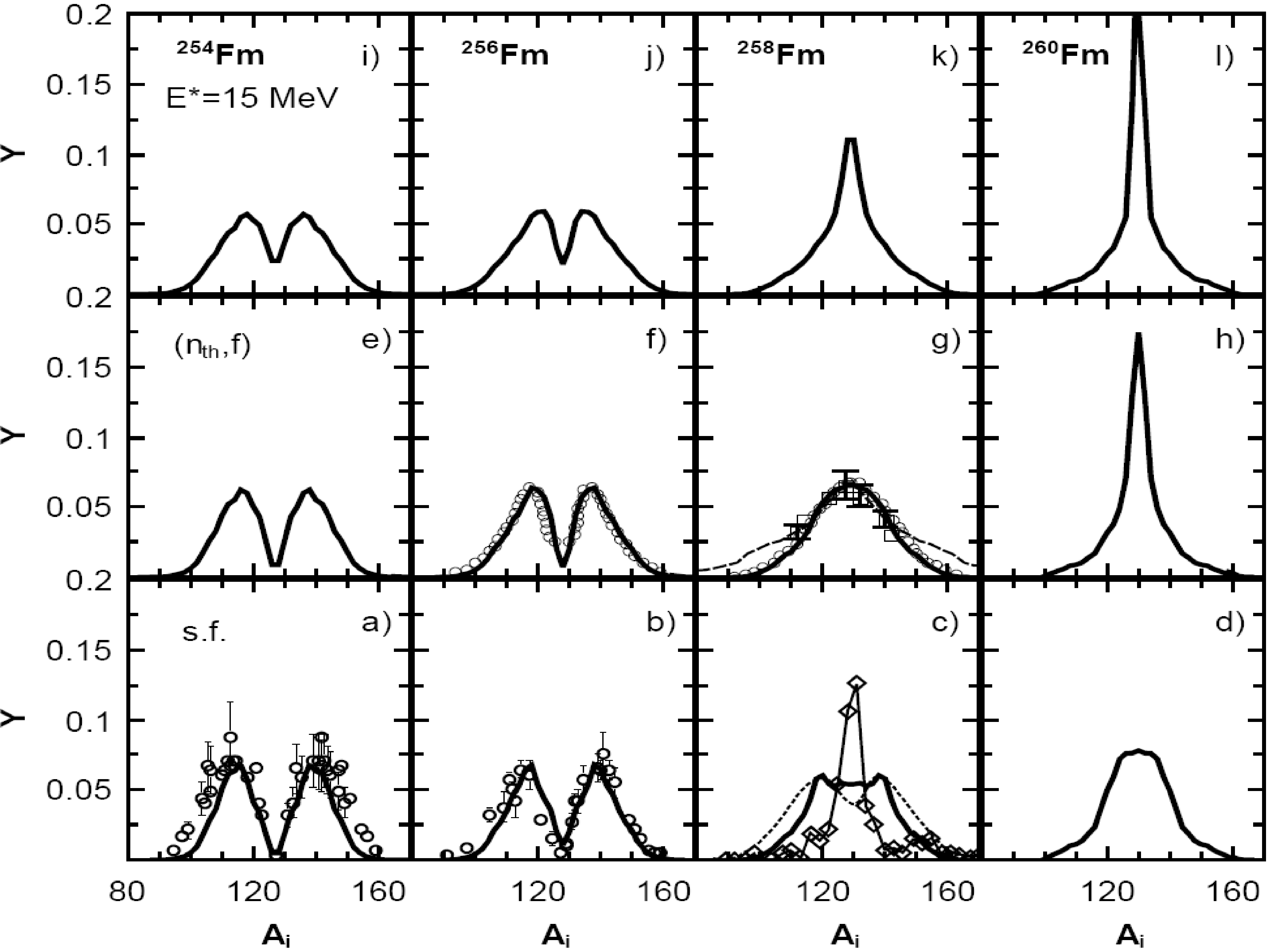

^{254}Fm
^{256}Fm
^{258}Fm
^{260}Fm
E*=15 MeV
(n$_{th}$,f)
s.f.
i)
j)
k)
l)
e)
f)
g)
h)
a)
b)
c)
d)
Y
0.2
0.15
0.1
0.05
80
120
160
A_i

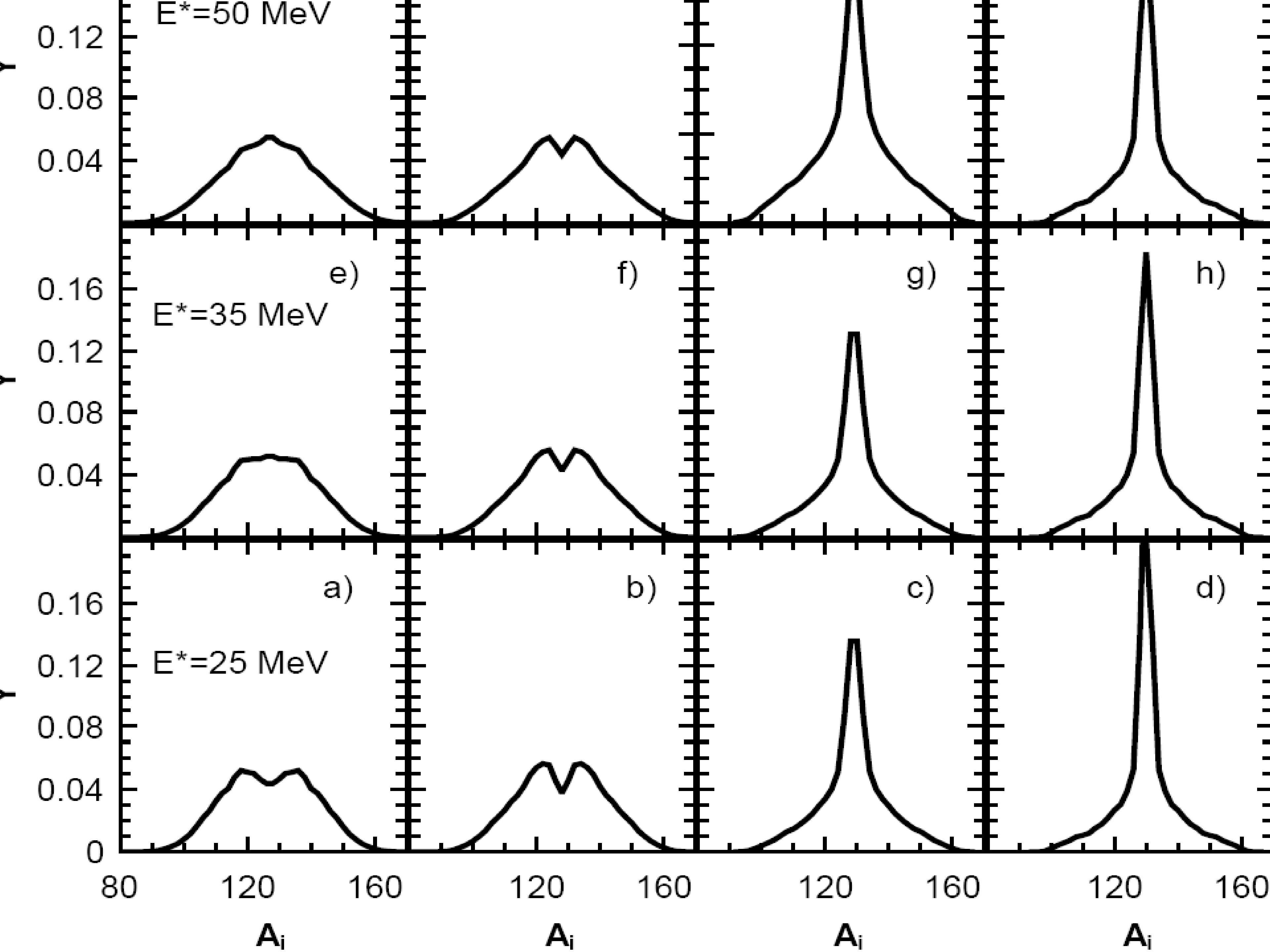

E*=50 MeV
E*=35 MeV
E*=25 MeV
e)
f)
g)
h)
a)
b)
c)
d)
Y
0.12
0.08
0.04
0.16
0
80
120
160
A_i

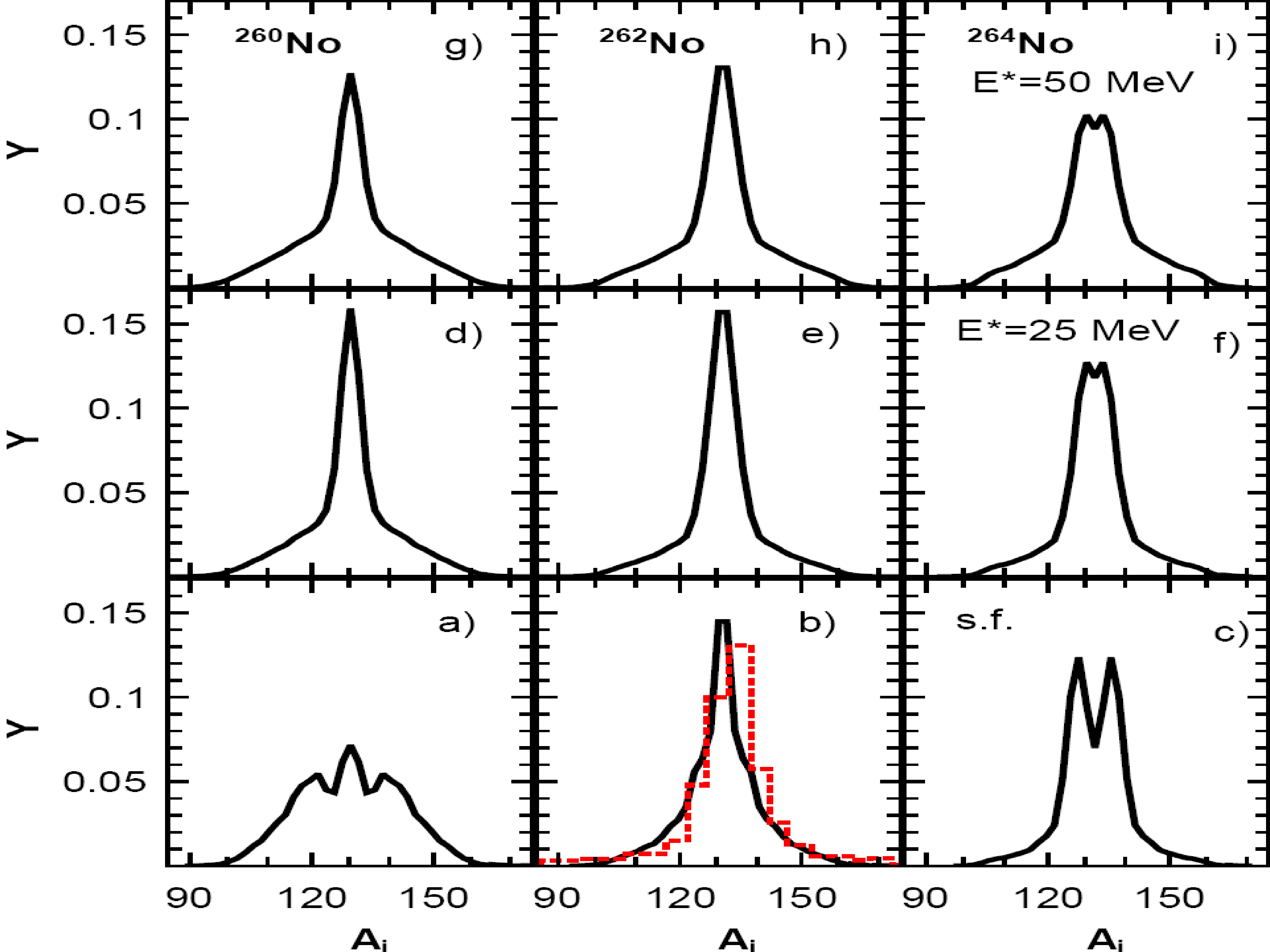

^{260}No
g)
^{262}No
h)
^{264}No
i)
E*=50 MeV
d)
e)
E*=25 MeV
f)
a)
b)
s.f.
c)
Y
0.15
0.1
0.05
90
120
150
A_i

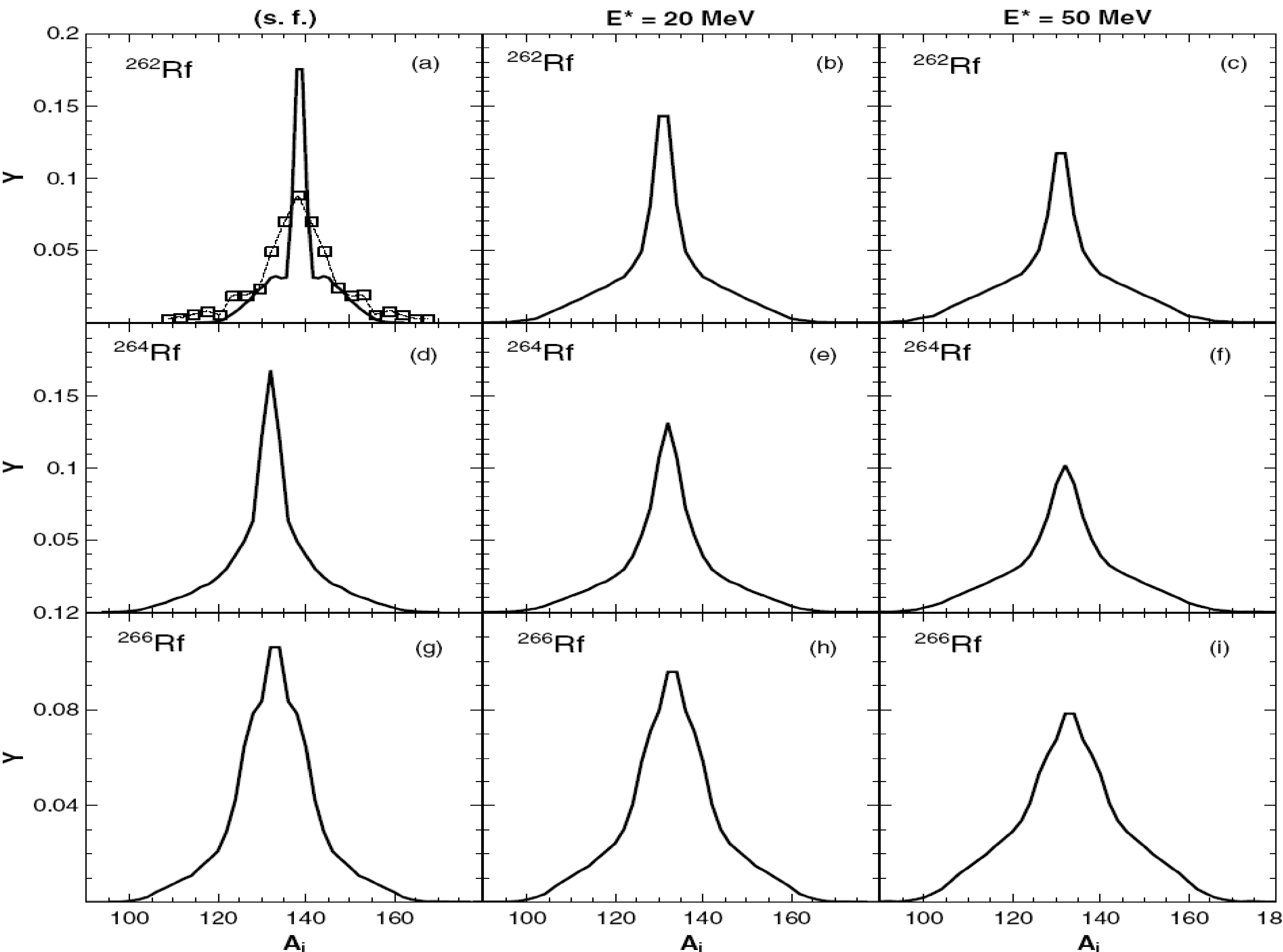
(s. f.)
E* = 20 MeV
E* = 50 MeV
^{262}Rf (a)
^{262}Rf (b)
^{262}Rf (c)
^{264}Rf (d)
^{264}Rf (e)
^{264}Rf (f)
^{266}Rf (g)
^{266}Rf (h)
^{266}Rf (i)
Y
0.2
0.15
0.1
0.05
0.12
0.08
0.04
100
120
140
160
180
A_i

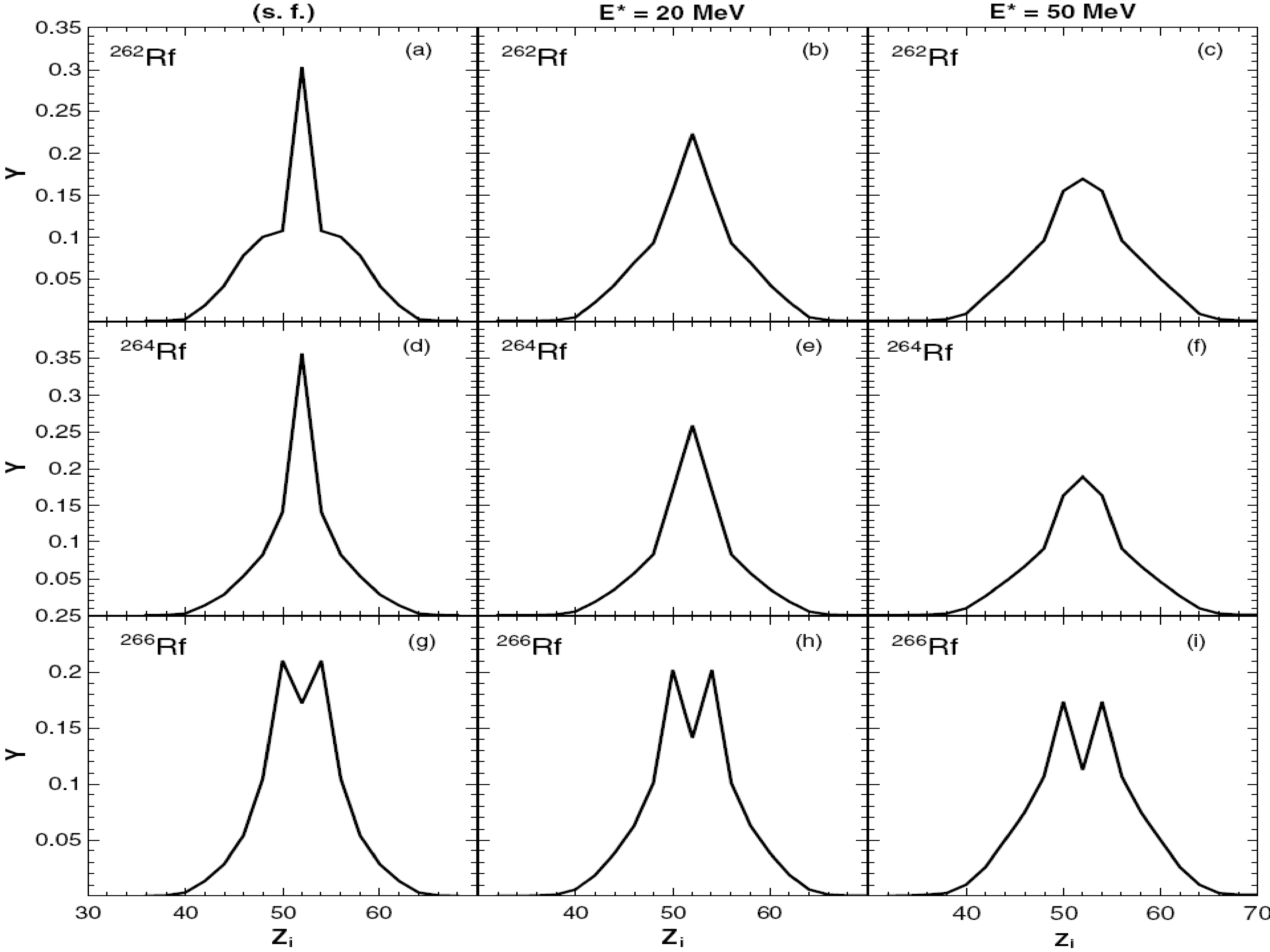

(s. f.)
E* = 20 MeV
E* = 50 MeV
Y
Y
Y
^{262}Rf (a)
^{262}Rf (b)
^{262}Rf (c)
^{264}Rf (d)
^{264}Rf (e)
^{264}Rf (f)
^{266}Rf (g)
^{266}Rf (h)
^{266}Rf (i)
Z_i
Z_i
Z_i

Experimental verifications of this unexpected difference between mass and charge distributions are desirable

The change of charge/mass-yields with increasing isospin or excitation energy is related to the change of PES at scission point

Potential energy at scission is main ingredient

1) **Liquid-drop energy** globally increases when mass number deviate from symmetry.
2) **Interaction energy** has the opposite behavior.
3) **Both** depend on deformations of nuclei: larger deformations result in smaller interaction energy, larger liquid-drop energy.
4) **Deformations** depend on shell effect: **magic** nuclei are expressed in small deformations.
5) **Shell correction energy**

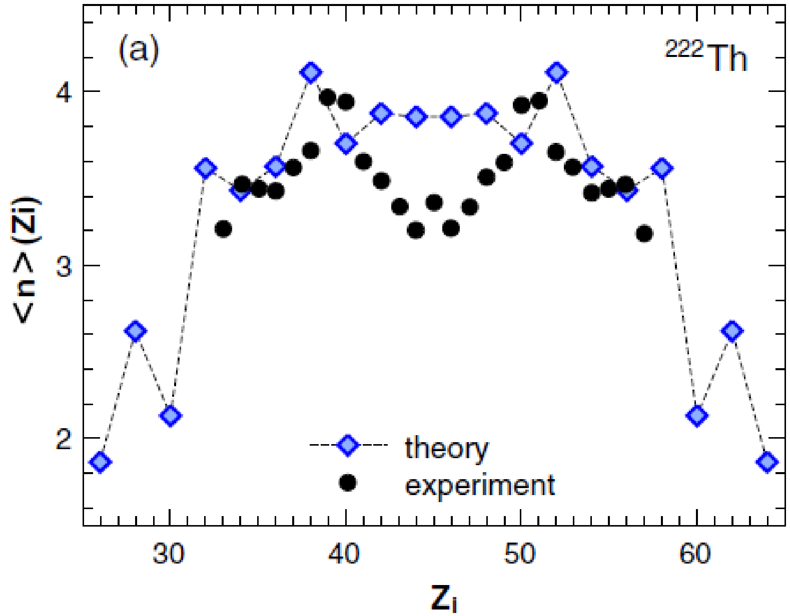

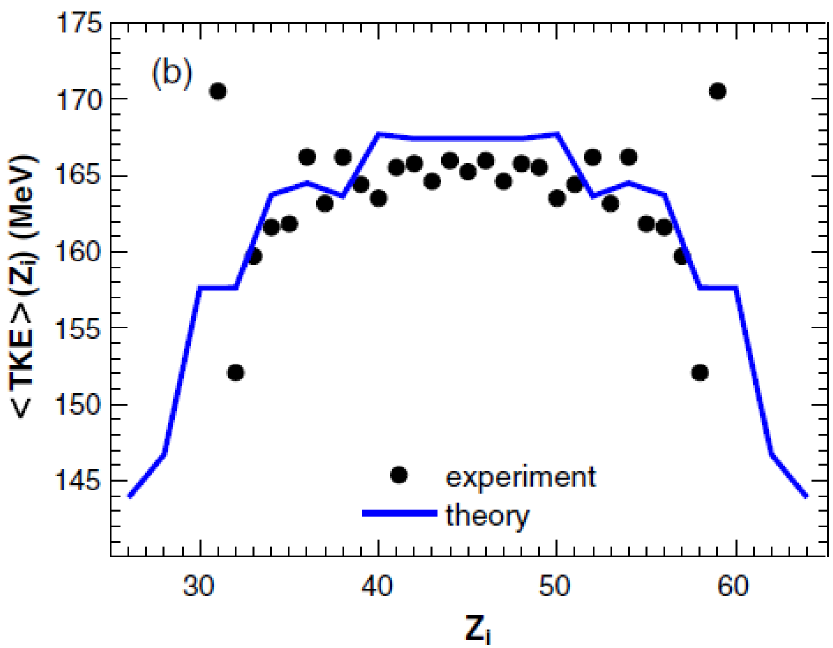

The calculated (lines) and experimental (closed symbols) neutron multiplicity (a) and TKE (b) distributions for electromagnetic induced fission of ^{222}Th at 11 MeV excitation energy.

$Z_1 \times Z_2$

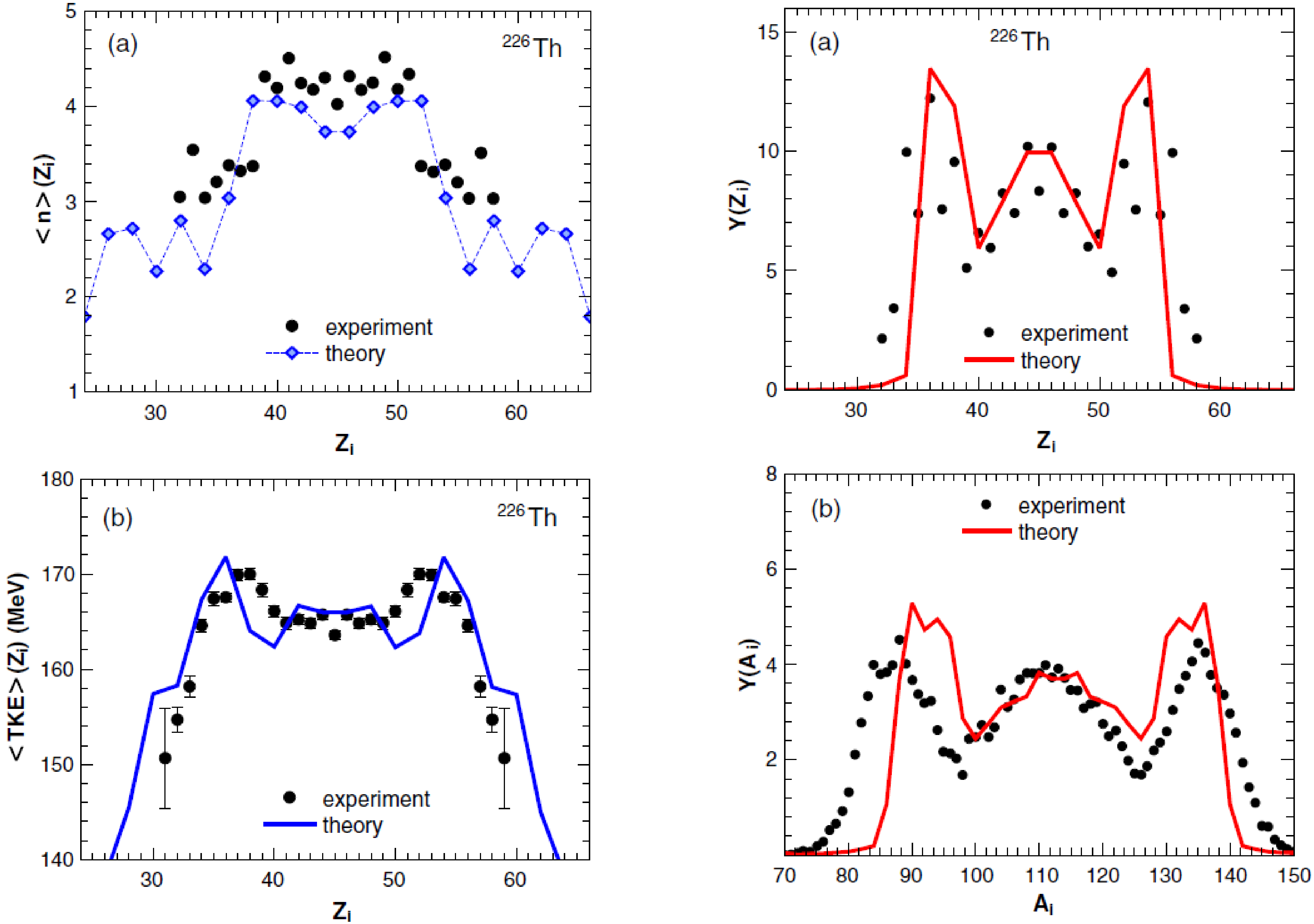

Electromagnetic induced fission of ^{226}Th at 11 MeV excitation energy.

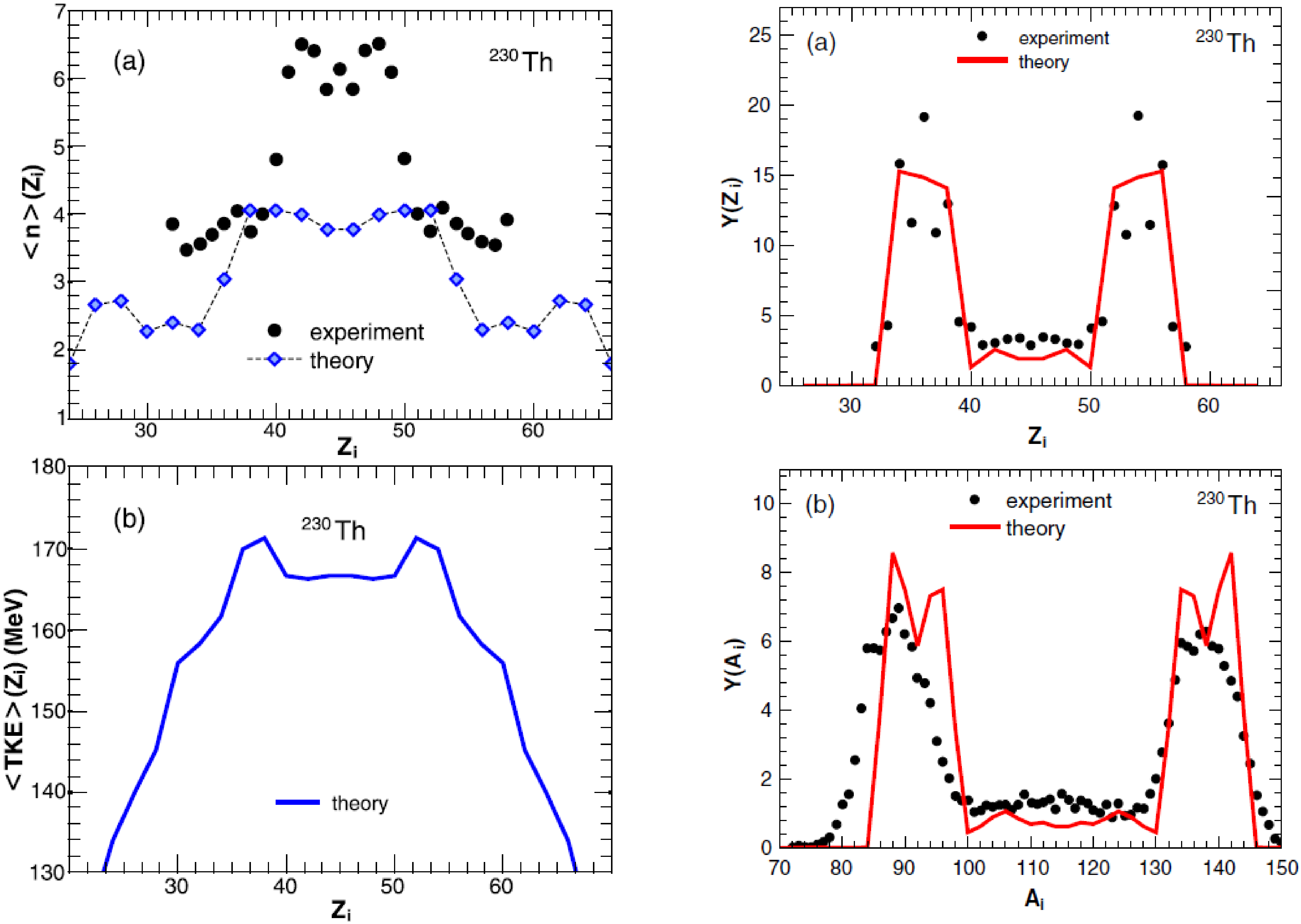

Electromagnetic induced fission of ^{230}Th at 11 MeV excitation energy.

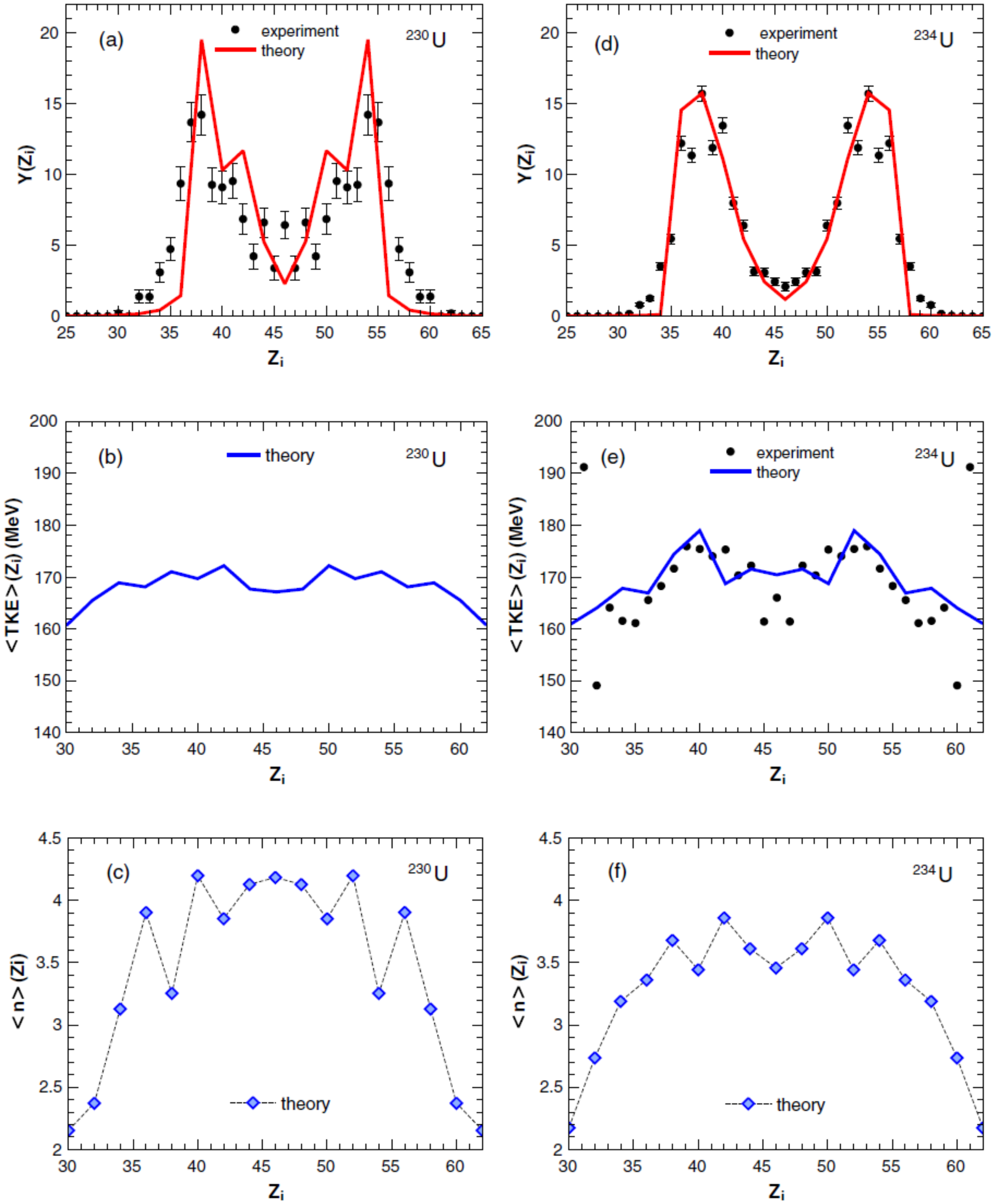

The calculated (lines) and experimental (closed symbols) [NPA **665**, 221 (2000); **693**, 169 (2001); **368**, 319 (1981)] charge [(a), (d)], TKE [(b), (e)], and neutron multiplicity [(c), (f)] distributions of fission fragments for electro-magnetic induced fission of ^{230,234}U at 11 MeV excitation energy. The lines connect the calculated points for even-even fission fragments.

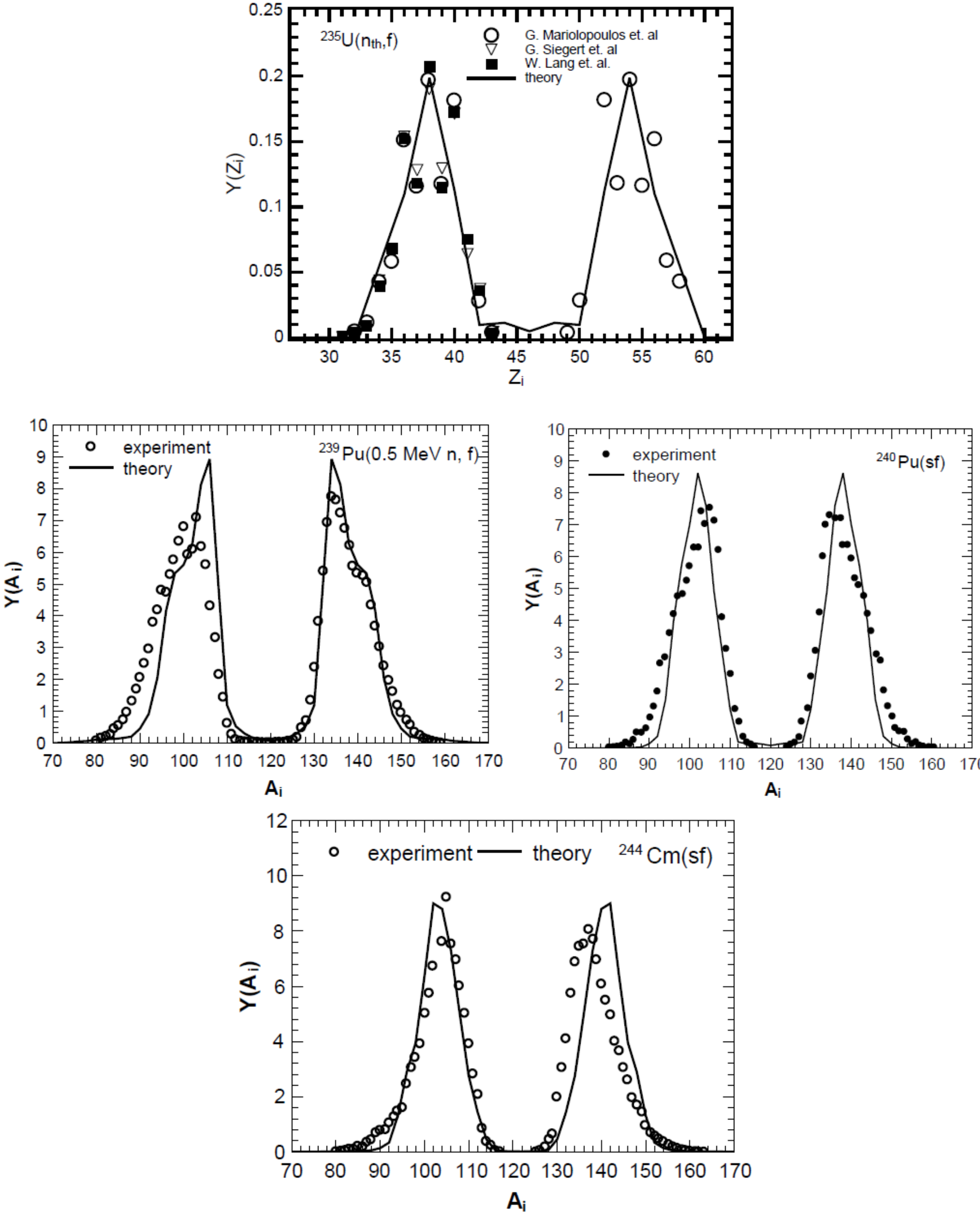

235U(nth,f)
G. Mariolopoulos et. al
G. Siegert et. al
W. Lang et. al.
theory
Y(Zi)
Zi
experiment
theory
239Pu(0.5 MeV n, f)
Y(Ai)
Ai
experiment
theory
240Pu(sf)
Y(Ai)
Ai
experiment
theory
244Cm(sf)
Y(Ai)
Ai

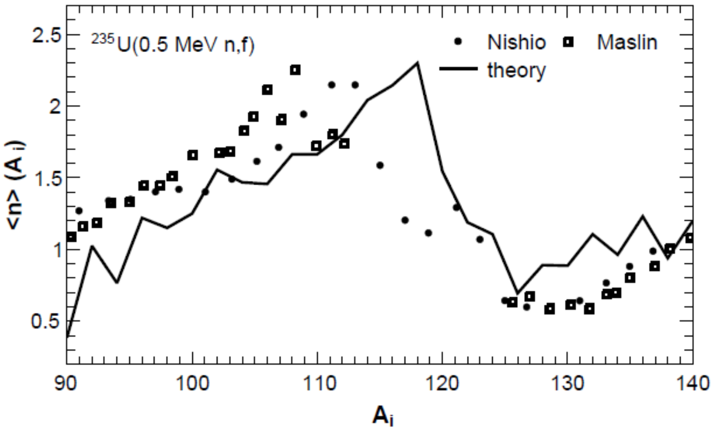
^{235}U(0.5 MeV n,f)
Nishio
Maslin
theory
<n> (A i)
A i

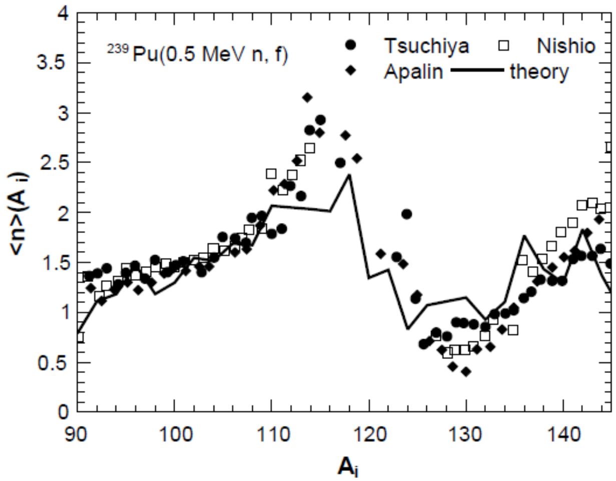
^{239}Pu(0.5 MeV n, f)
Tsuchiya
Nishio
Apalin
theory
<n>(A i)
A i

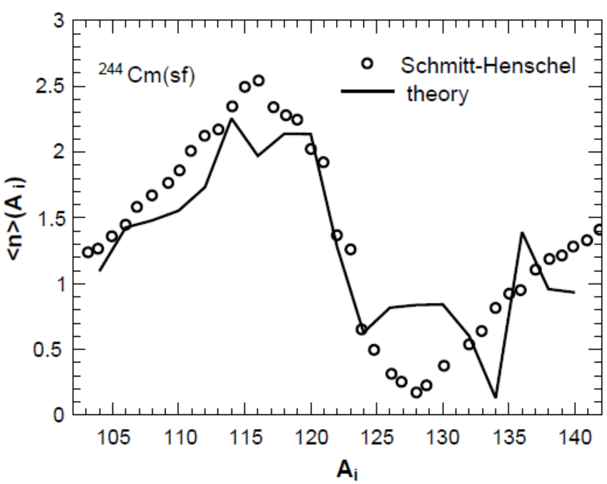
^{244}Cm(sf)
Schmitt-Henschel
theory
<n>(A i)
A i

The probability of evaporating exactly *x* neutrons from the excited fragment "*i*" with excitation energy E^*_i

$$
\begin{aligned}
P_{xn}(E_i^*) &= P(x) - P(x+1), \\
P(x) &= 1 - e^{-\Delta_x} \left(1 + \sum_{k=1}^{2x-3} \frac{(\Delta_x)^k}{k!} \right), \\
P(x+1) &= 1 - e^{-\Delta_{x+1}} \left(1 + \sum_{k=1}^{2x-1} \frac{(\Delta_{x+1})^k}{k!} \right),
\end{aligned}
$$

$\Delta_x = \left(E_i^* - \sum_{k=1}^{x} B_k\right)/T_i$, where B_k is the experimental neutron binding energy at the k-th evaporation step and $T_i = (E_i^*/a_i)^{1/2}$ is the temperature.

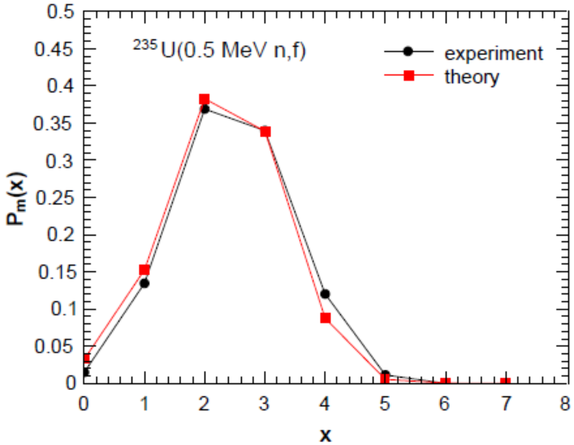

The calculated (squares connected by lines) and experimental (open circles connected by lines) [PR **101**, 1012 (1956); BNL-NCS-35513 (1985); Nucl. Sci. Eng. **86**, 315 (1984)] probabilities $P_m(x)$ as functions of multiplicity x for the indicated fission reactions.

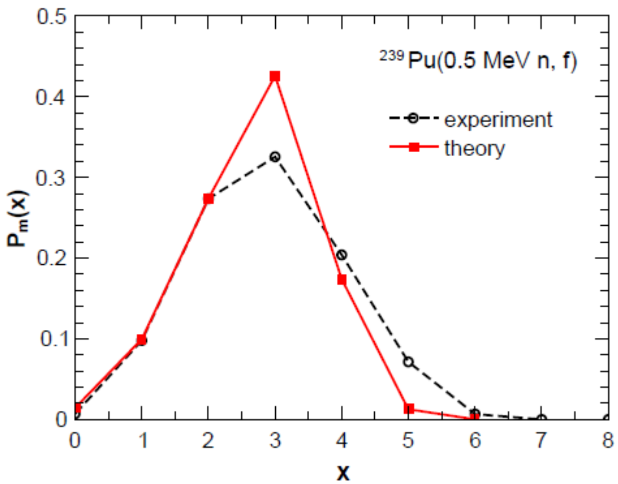

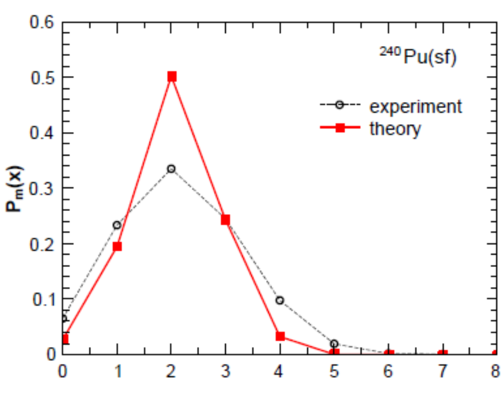

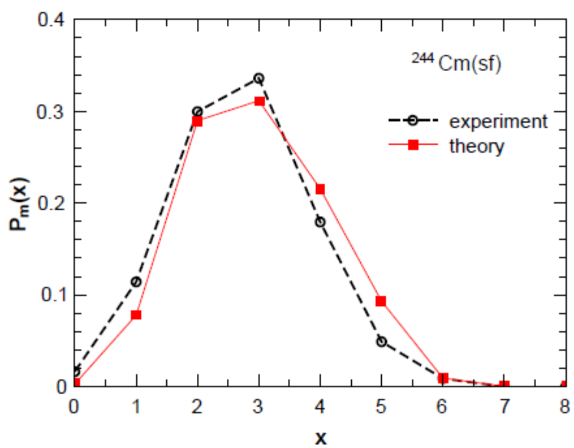

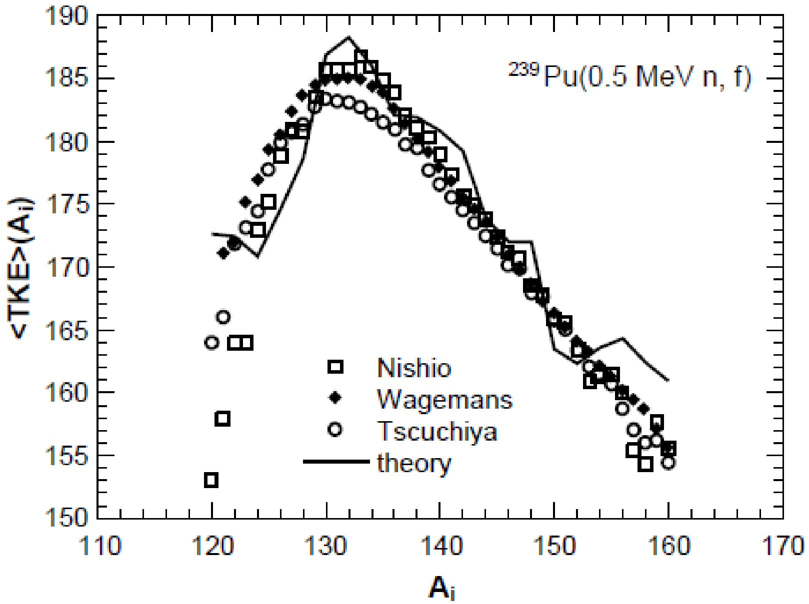

^{239}Pu(0.5 MeV n, f)
Nishio
Wagemans
Tscuchiya
theory
<TKE>(A$_i$)
A$_i$

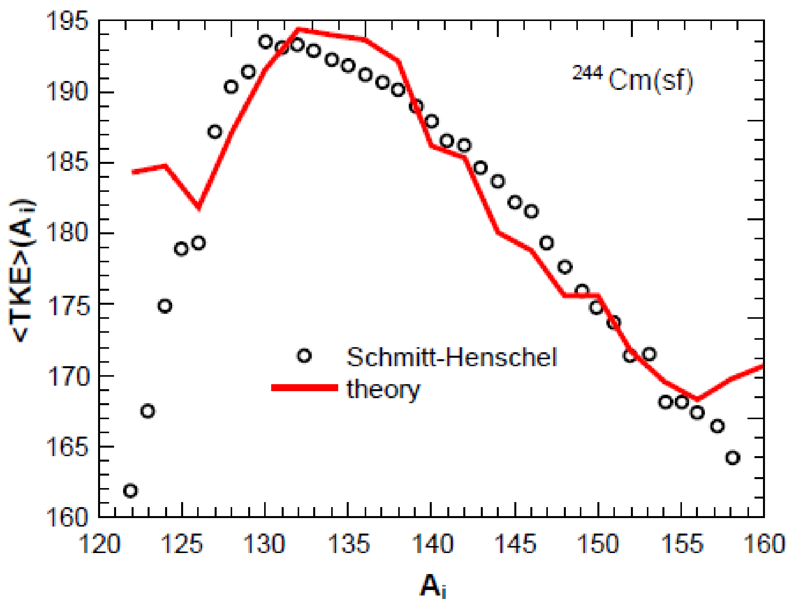

^{244}Cm(sf)
Schmitt-Henschel
theory
<TKE>(A$_i$)
A$_i$

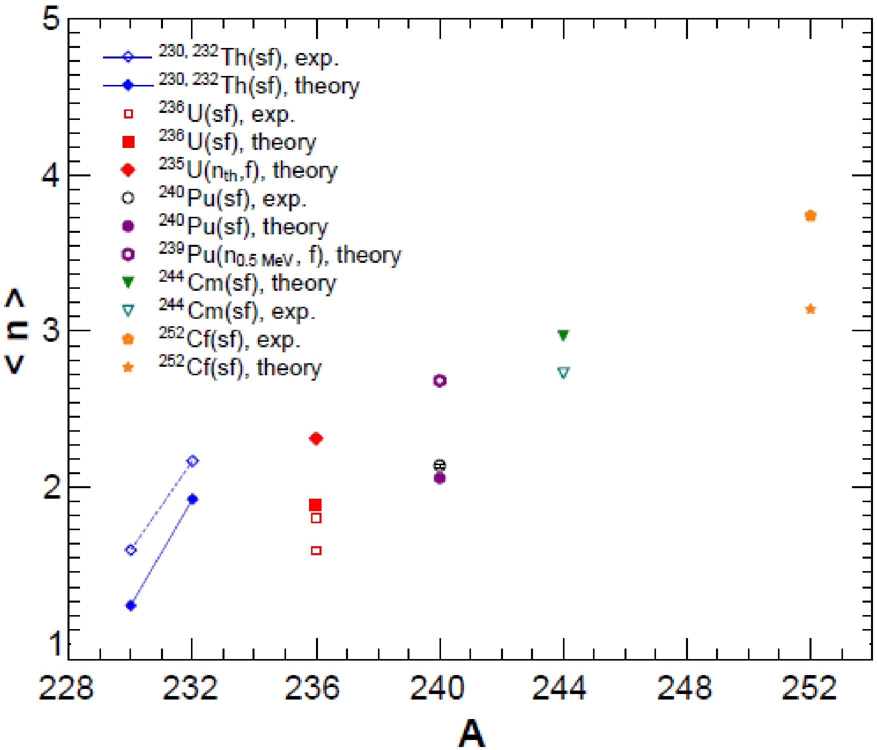

The calculated (open symbols) and experimental (closed symbols) average numbers of neutrons $\langle n \rangle$ emitted per act of fission as functions of the mass number A of indicated fissioning nucleus.

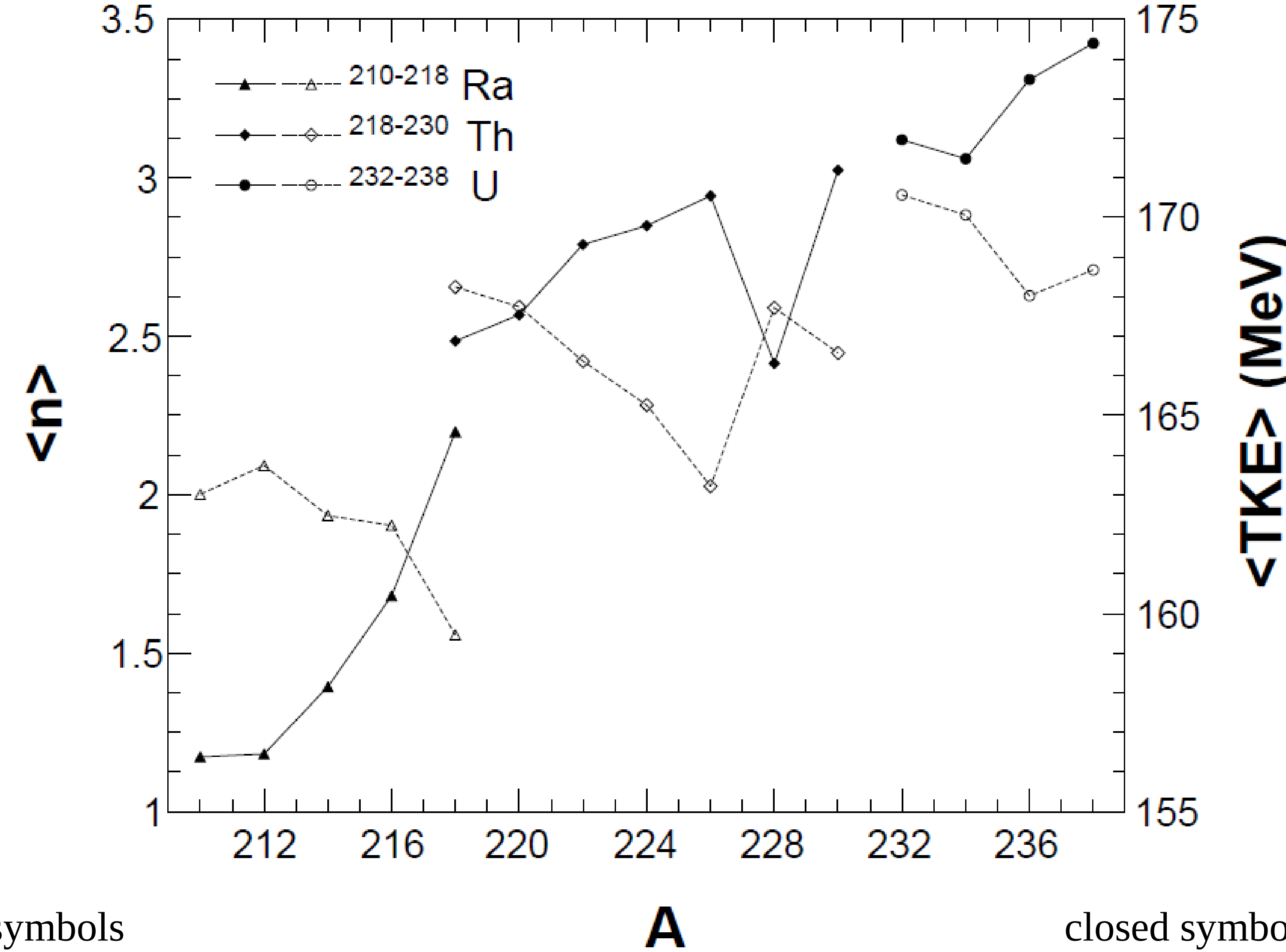

open symbols

closed symbols

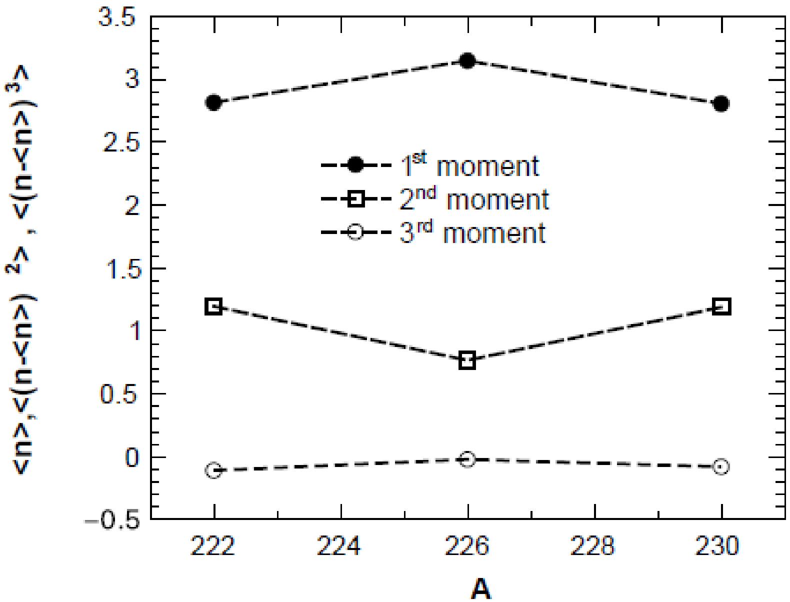

$^{222,226,230}\mathrm{Th}\ (E^{*} = 11\ \mathrm{MeV})$

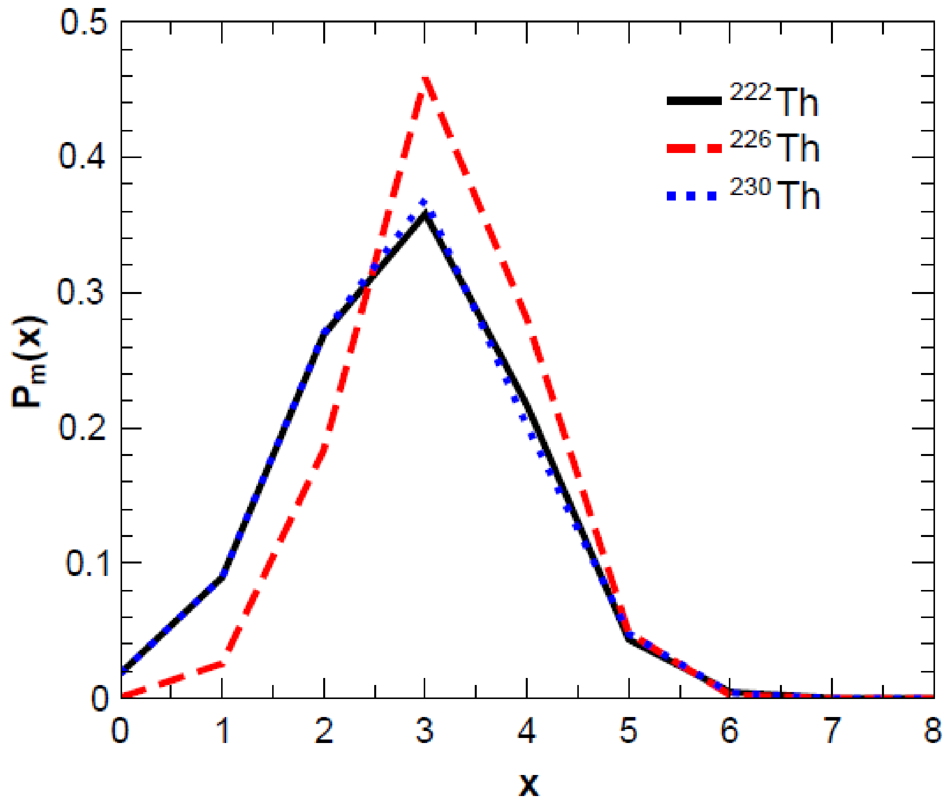

Minima in potential (maxima in yields) are direct result of interplay between liquid-drop, interaction, shell correction energies.

- **Shell effects** affect indirectly (through deformations) appearance of minima of PES, facilitation of large number of magic fragments.

As E* increases, shell & stiffness diminish, shifting minima on PES towards larger deformations and widening minima.

Direct role of **shell effects** is expressed by their ability to enhance or suppress formation of minima of PES.

Saturation effect

At some critical excitation energy saturation of symmetric yields occurs.

Further increase of E^* leads only to population of more asymmetric accessible configurations.

It is worth to be studied experimentally

- **Transition from the symmetric to the asymmetric fission in the Th isotopes influences <*n*>, <*TKE*>, and $P_m(x)$. These values can serve as markers to identify such transitions.**

- **The same can be observed in the transition from asymmetric fission of ^{254,256}Fm (^{252}No) to symmetric one of ^{258,260}Fm (^{258,262}No).**

Thank You For Your Attention！

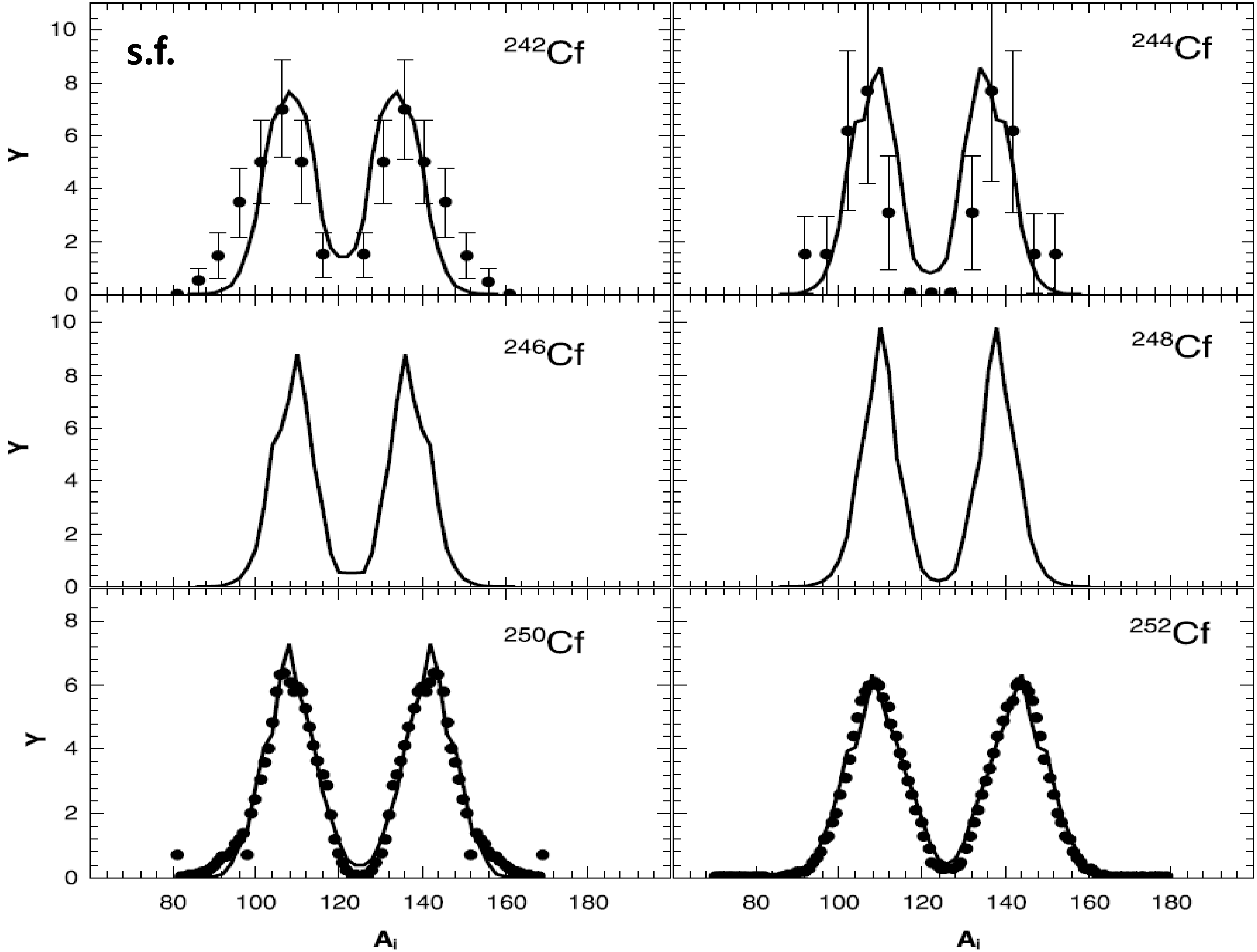

s.f.
242Cf
244Cf
246Cf
248Cf
250Cf
252Cf
Y
Y
Y
0
2
4
6
8
10
80
100
120
140
160
180
Ai
Ai

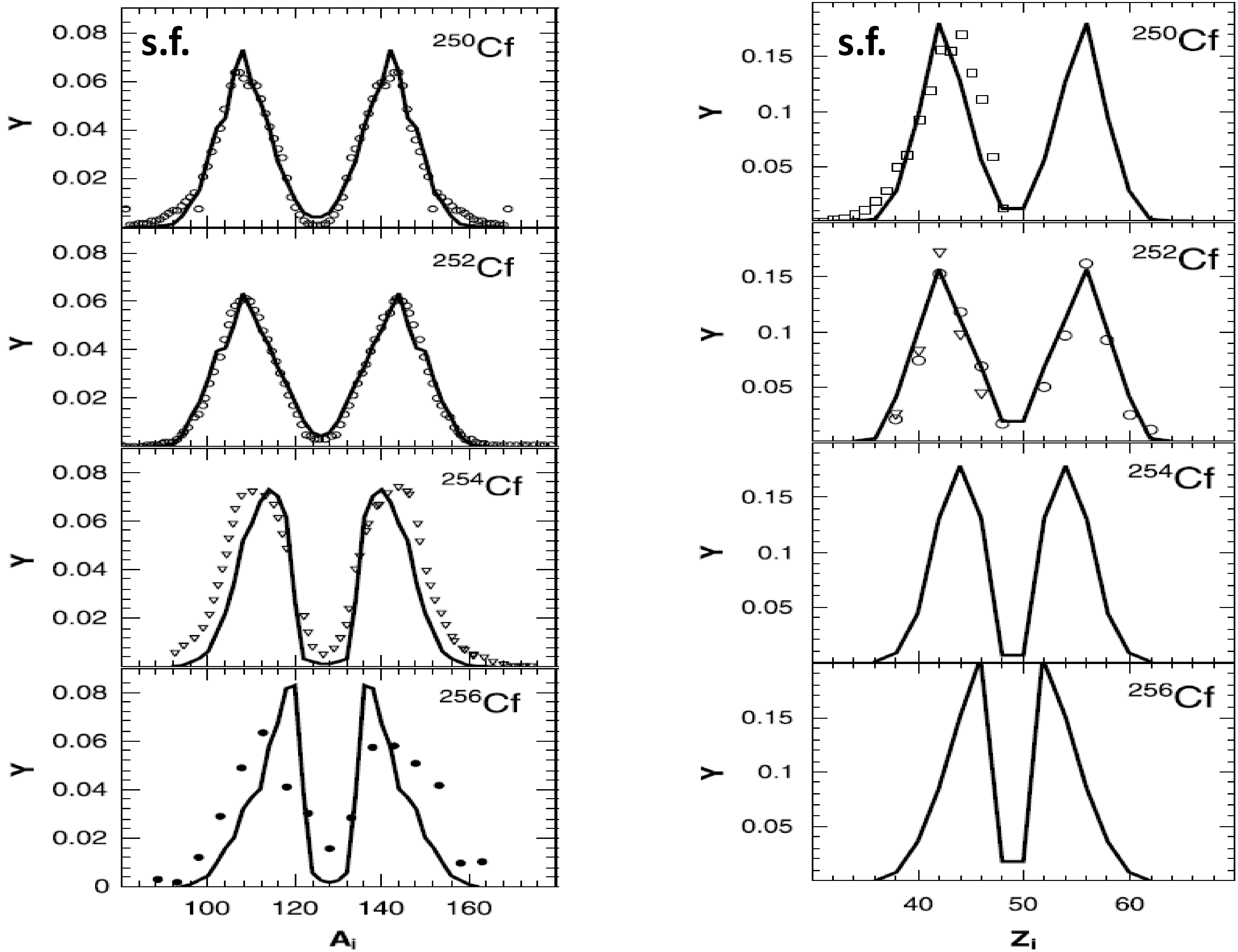

s.f.
250Cf
252Cf
254Cf
256Cf
Y
0.08
0.06
0.04
0.02
0
100
120
140
160
Ai
s.f.
250Cf
252Cf
254Cf
256Cf
Y
0.15
0.1
0.05
40
50
60
Zi

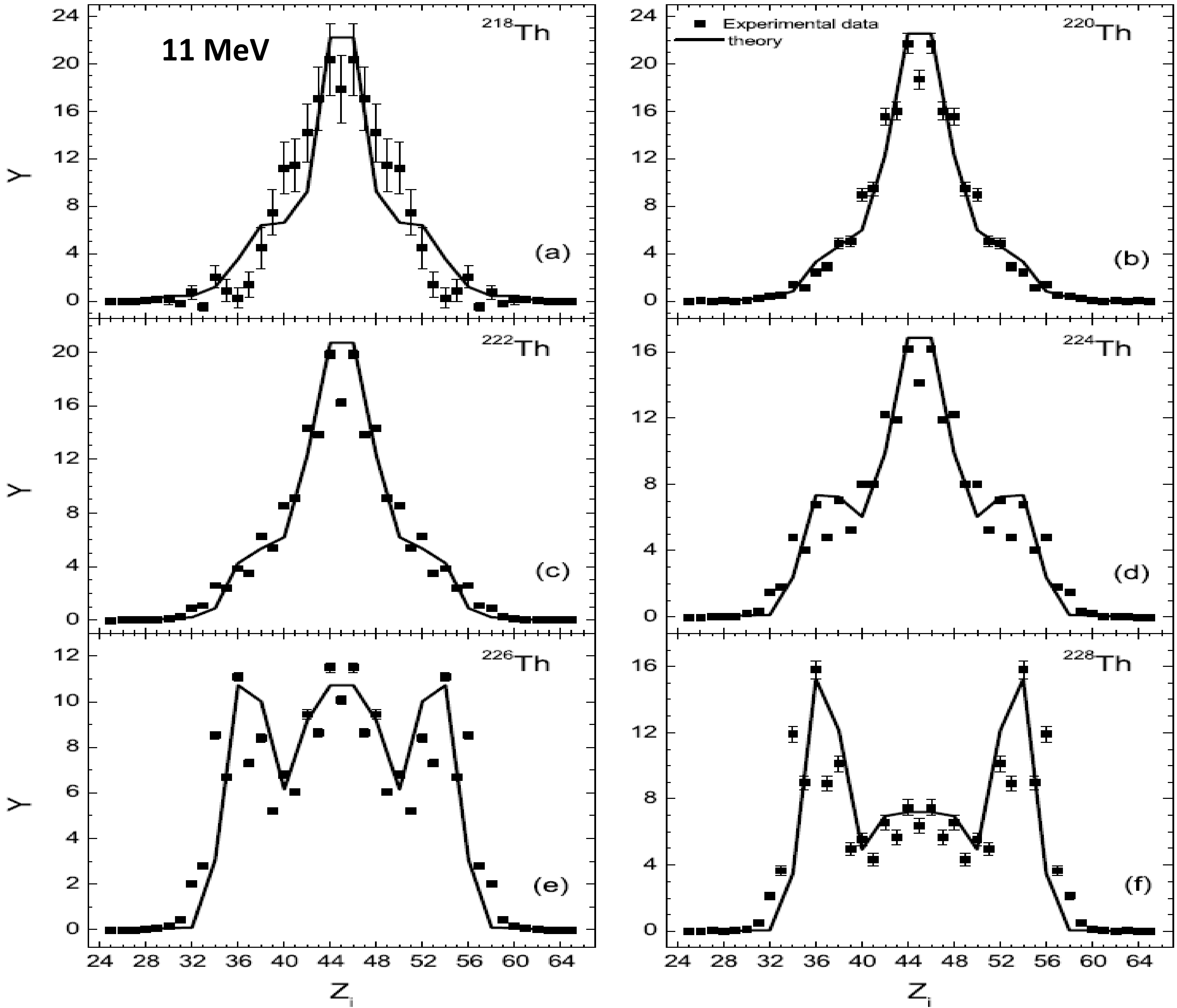

11 MeV
^{218}Th
^{220}Th
Experimental data
theory
^{222}Th
^{224}Th
^{226}Th
^{228}Th
(a)
(b)
(c)
(d)
(e)
(f)
Y
Z_i

Exper.:K.Hirose et al.
PRL 119 (2017) 222501

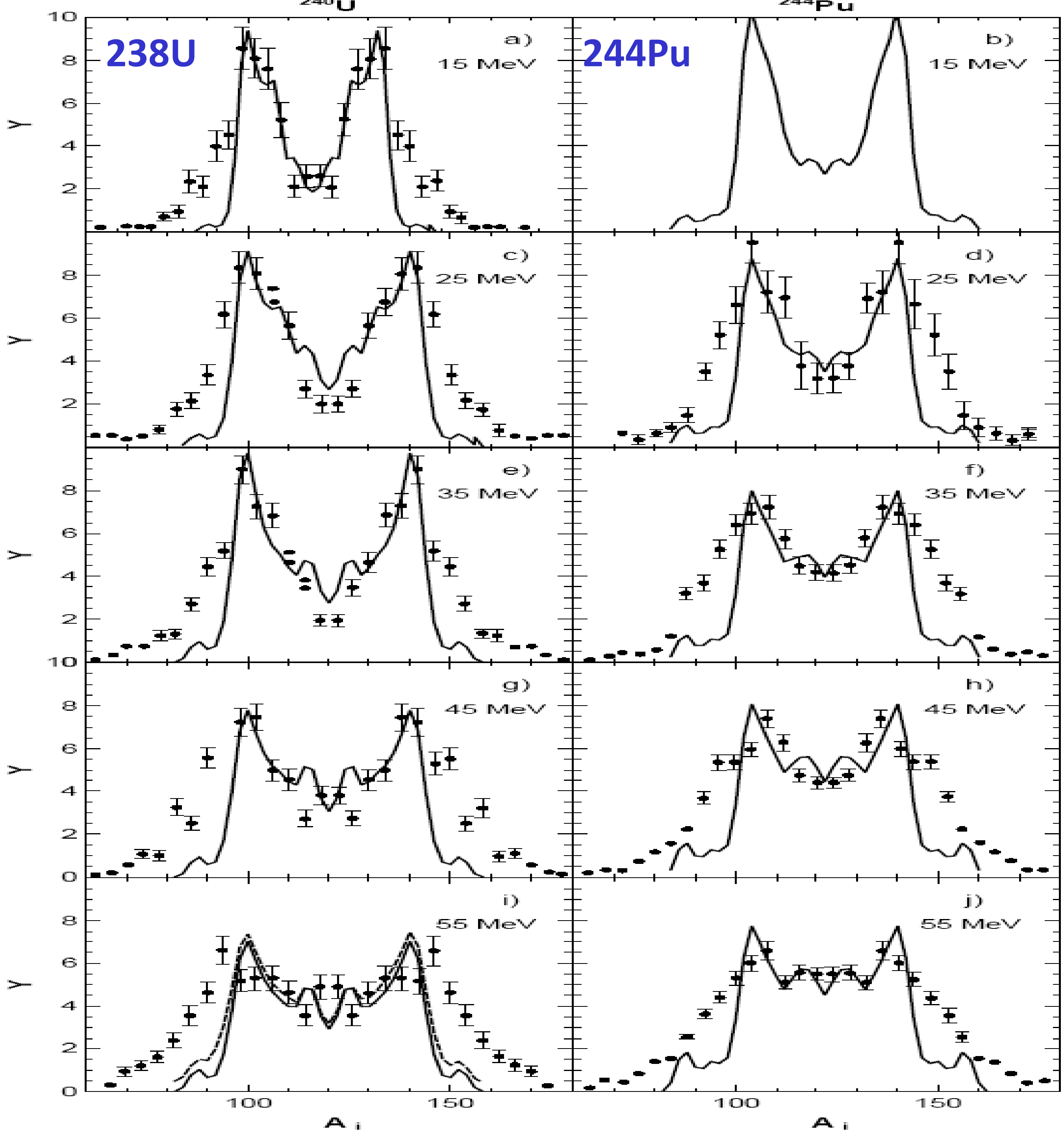

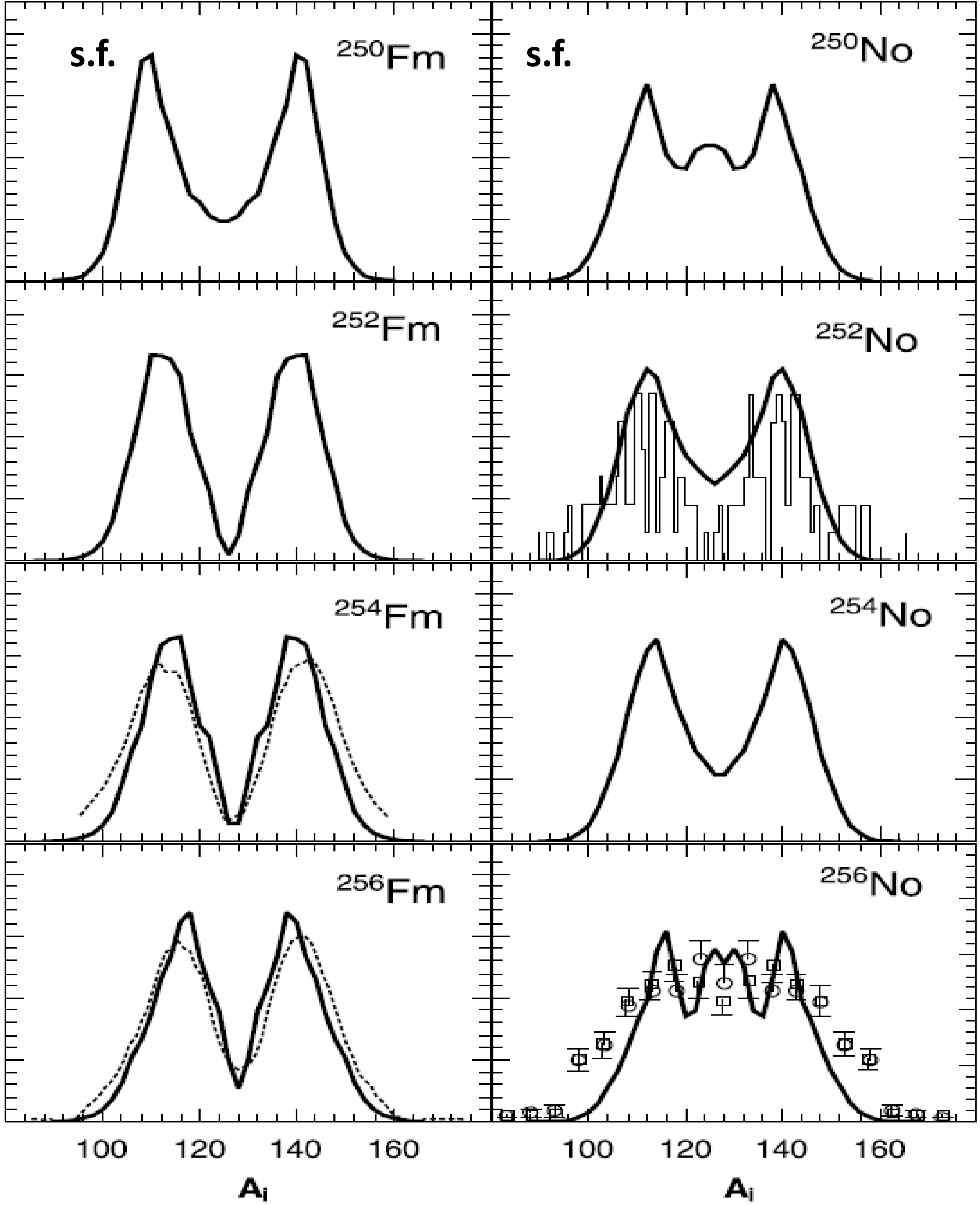

s.f.
^{250}Fm
s.f.
^{250}No
^{252}Fm
^{252}No
^{254}Fm
^{254}No
^{256}Fm
^{256}No
100
120
140
160
A_i
100
120
140
160
A_i

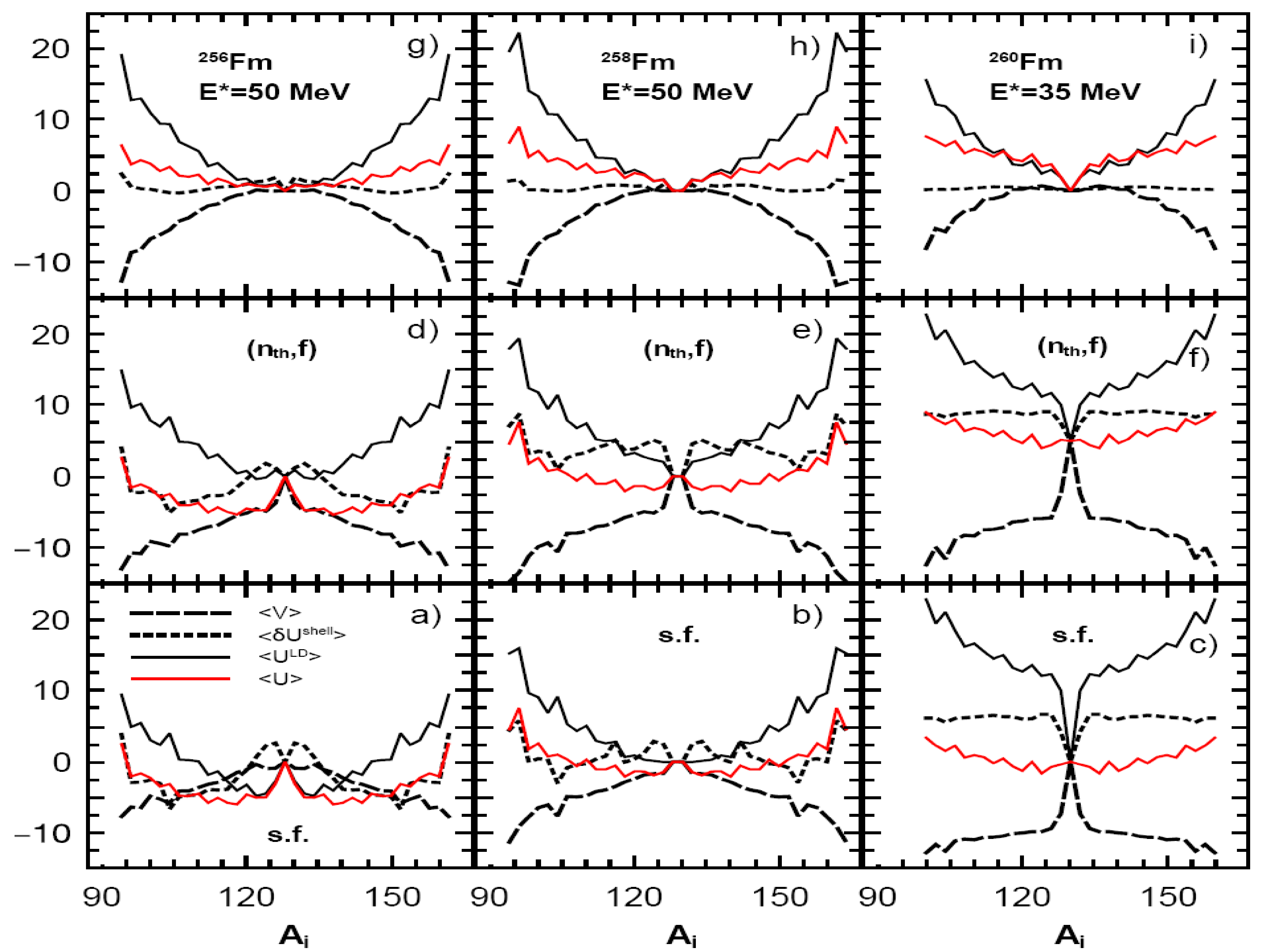

^{256}Fm
E*=50 MeV
g)
^{258}Fm
E*=50 MeV
h)
^{260}Fm
E*=35 MeV
i)
(n$_{th}$,f)
d)
(n$_{th}$,f)
e)
(n$_{th}$,f)
f)
<V>
<δU^{shell}>
<U^{LD}>
<U>
a)
s.f.
s.f.
b)
s.f.
c)
20
10
0
−10
90
120
150
A$_i$

Model

<ins>*Coordinates Z_1, A_1, β_i (i=1,2), R completely describe the geometry of system.*</ins>

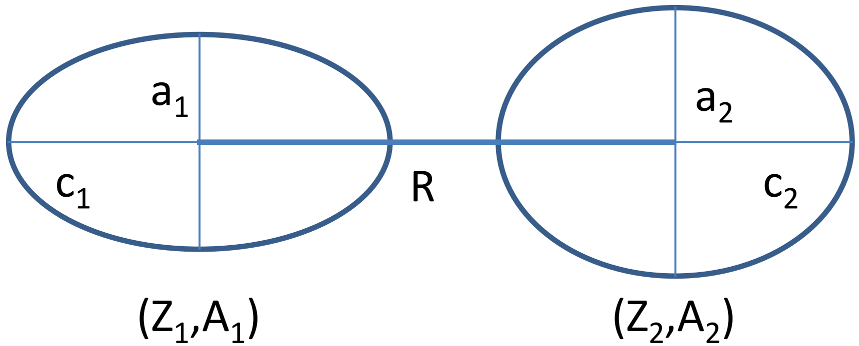

<ins>*The interaction potential between fragments is:*</ins>

$$V(R, Z, A, J, \beta_1, \beta_2) = V_N + V_C$$

$$V_c(R, Z_1, Z_2, \beta_1, \beta_2) = \frac{e^2 Z_1 Z_2}{R} + \left(\frac{9}{20\pi}\right)^{1/2} \frac{e^2 Z_1 Z_2}{R^3} \sum_{i=1}^{2} R_i^2 \beta_i \left[1 + \frac{2}{7}\left(\frac{5}{\pi}\right)^{1/2} \beta_i\right] P_2(cos\theta_i)$$

$$V_N = \int \rho_1(r_1)\rho_2(R - r_2)F(r_1 - r_2)dr_1 dr_2$$

$$F(r_1 - r_2) = C_0[F_{in}\frac{\rho_1(r_1)}{\rho_{00}} + F_{ex}(1 - \frac{\rho_1(r_1)}{\rho_{00}})]\delta(r_1 - r_2)$$

$$\rho_0(r) = \rho_1(r) + \rho_2(R - r)$$

$$F_{in,ex} = f_{in,ex} + f'_{in,ex}\frac{(N - Z)(N_2 - Z_2)}{(N + Z)(N_2 + Z_2)}$$

$$C_0 = 300 MeV fm^3$$

$$f_{in} = 0.09, f_{ex} = -2.59$$

$$\rho_{00} = 0.17 fm^{-3}, a = 0.51 - 0.56 fm$$

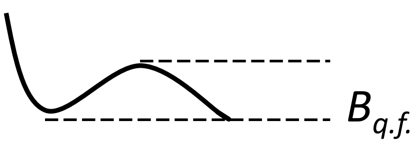

Sh.A. Kalandarov, G.G. Adamian, N.V. Antonenko, W. Scheid, Phys. Rev. C 82, 044603 (2010)

Model

- ***The total energy:***

$$U(A_i, Z_i, \beta_i, d) =$$
$$=U_{macro}(A_i, Z_i, \beta_i, d) + \delta U^{shell}(A_i, Z_i, \beta_i) =$$
$$= \sum_{i=1,2} U_i^{LD}(A_i, Z_i, \beta_i) + \sum_{i=1,2} \delta U_i^{shell}(A_i, Z_i, \beta_i', E_i^*) +$$
$$+V_N(A_i, Z_i, \beta_i, d) + V_C(A_i, Z_i, \beta_i, d).$$

$$U_i^{L.D.}(A_i, Z_i, \beta_i) = U_i^{Surface}(A_i, Z_i, \beta_i) + U_i^C(A_i, Z_i, \beta_i) + U_i^{Sym}(A_i, Z_i)$$

- ***Liquid drop terms:***

$$U_i^{sym}(A_i, Z_i) = 27.612 \frac{(N_i - Z_i)^2}{A_i}$$

$$U_i^C(A_i, Z_i, \beta_i) = \frac{3}{5} \frac{(Z_i e)^2}{R_{0,i}} \frac{\beta_i^{1/3}}{\sqrt{\beta_i^2 - 1}} ln(\beta_i + \sqrt{\beta_i^2 - 1})$$

J. Maruhn and W. Greiner, Z. Phys. ***251****, 431 (1972).*

Model

Surface energy with variable surface tension:

$$U_i^{Surface}(A_i, Z_i, \beta_i) = \sigma_i S_i$$

$$\sigma_i = \sigma_{0,i}(1 + k_i(\beta_i - \beta_i^{g.s.})^2)$$

$$\sigma_{0,i} = 0.9517(1 - 1.7826((N_i - Z_i)^2)/A_i)^2)$$

$$k_i = \frac{1}{1+exp[-0.063(C_{vib}(Z_i, A_i) - 67)]}$$

$$C_{vib}(Z_i, A_i) = \frac{\hbar\omega_{vib}^i(3Z_i e R_{0,i}^2/(4\pi))^2}{2B(E2)_{vib}^i}$$

$$B(E2)_{vib} = E_{2+}^i B(E2)_{rot}^i/(\hbar\omega_{vib}^i)$$

Excitation energy: of the scission configuration can be calculated as a sum of the initial excitation energy of the fissioning nucleus and the difference of the potential energies of the fissioning nucleus and scission configuration:

$$E^*(A_i, Z_i, \beta_i, R_m) = E_{CN}^* + [U_{CN}(A, Z, \beta) - U(A_i, Z_i, \beta_i, R_m)]\,.$$

$$T_{DNS}(E^*) = \sqrt{E^*/a}\ \ , a = A/12\, MeV^{-1}$$

Temperature dependence of LD terms:

$$U_i^{sym}(A_i, Z_i, T) = U_i^{sym}(A_i, Z_i, T = 0)(1 + 0.5 * 10^{-4}T^2),$$

$$U_i^C(A_i, Z_i, \beta_i, T) = U_i^C(A_i, Z_i, \beta_i, T = 0)(1 - 10^{-2}T^2)$$

$$U_i^{Surf}(A_i, Z_i, \beta_i, T) = U_i^{Surf}(A_i, Z_i, \beta_i, T = 0)(1 + 8.5 * 10^{-3}T^2).$$

$$k_i(E_i^*) = k_i * exp\,[-E_i^*/E_k]$$

Shell damping:

$$\delta U_i^{shell}(A_i, Z_i, \beta_i', E_i^*) = \delta U_i^{shell}(A_i, Z_i, \beta_i', E_i^* = 0)exp[-E_i^*/E_D]$$

G. Sauer, H. Chandra, U. Mosel, Nucl. Phys. A ***264*** *(1976) 221-243*

Model

Yields:

Using
$$P_{Z,A}(E^*_{CN}, \beta_1, \beta_2) \sim exp\{-U(R_m, Z, A, \beta_1, \beta_2)/T\}$$
$$P^{decay}_{Z,A,\beta_1,\beta_2} \sim exp\{-B_{qf}(Z, A, \beta_1, \beta_2)/T\}$$

$$w(A_i, Z_i, \beta_i, E^*) = N_0 exp[-\frac{U(A_i, Z_i, \beta_i, R_m) + B_{qf}(A_i, Z_i, \beta_i)}{T}]$$

The different yields can be calculate by integrating over the deformations:

$$Y(A_i, Z_i) = N_0 \int\int w(A_i, Z_i, \beta_1, \beta_2, E^*)\, \mathrm{d}\beta_1 \mathrm{d}\beta_2,$$

$$Y(A_i) = N_0 \sum_{Z_i} \int\int w(A_i, Z_i, \beta_1, \beta_2, E^*)\, \mathrm{d}\beta_1 \mathrm{d}\beta_2,$$

$$Y(Z_i) = N_0 \sum_{A_i} \int\int w(A_i, Z_i, \beta_1, \beta_2, E^*)\, \mathrm{d}\beta_1 \mathrm{d}\beta_2,$$

$$TKE(A_i, Z_i) = V_c(A_i, Z_i, \beta_1, \beta_2) + V_n(A_i, Z_i, \beta_1, \beta_2)$$

$$<TKE>(A_i) = \frac{\sum_{Z_i} \int TKE(A_i, Z_i, \beta_1, \beta_2)\, w(A_i, Z_i, \beta_1, \beta_2, E^*) d\beta_1 d\beta_2}{\sum_{Z_i} \int w(A_i, Z_i, \beta_1, \beta_2, E^*) d\beta_1 d\beta_2}$$

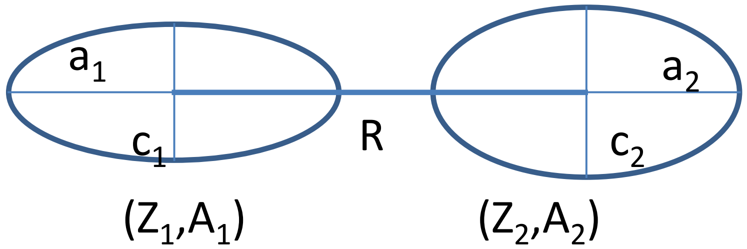

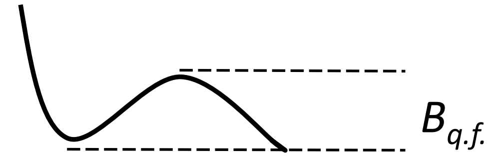

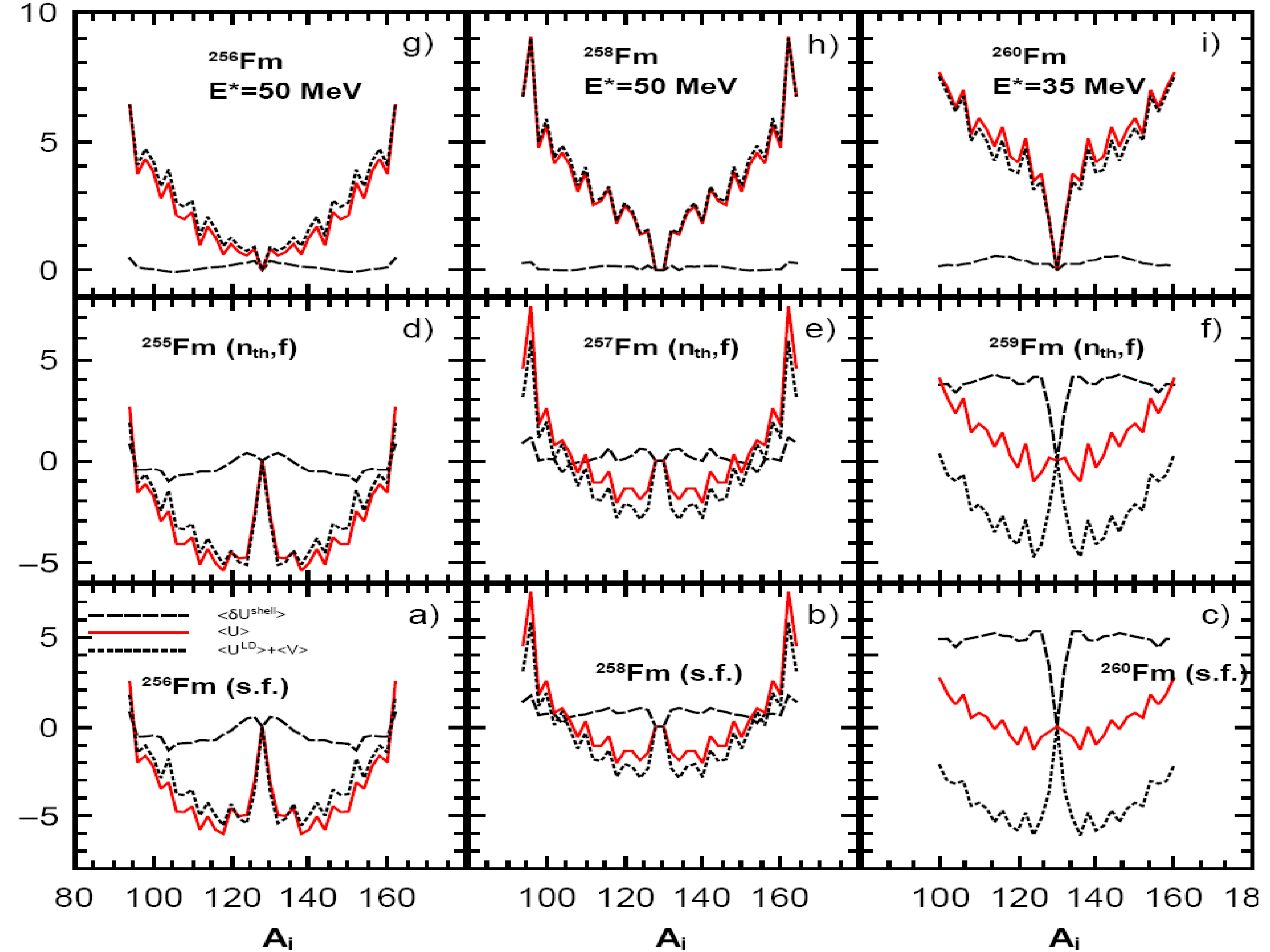

^{256}Fm
E*=50 MeV
g)
^{258}Fm
E*=50 MeV
h)
^{260}Fm
E*=35 MeV
i)
^{255}Fm (n_{th},f)
d)
^{257}Fm (n_{th},f)
e)
^{259}Fm (n_{th},f)
f)
<δU^{shell}>
<U>
<U^{LD}>+<V>
a)
^{256}Fm (s.f.)
b)
^{258}Fm (s.f.)
c)
^{260}Fm (s.f.)
A_i
A_i
A_i

For 260Fm(sf), for **130Sn+130Sn**, interaction and liquid-drop energies have opposite and almost canceling effects. Strong shell in **130Sn+130Sn** is seen. This also affects macro parts of potential by fixing minima at small deformations.

As E* increases, shell & stiffness diminish, shifting minima on PES [**130Sn+130Sn**] towards larger deformations. With increasing deformations **V** & **U** considerably decrease, mass yield becomes narrow.

Symmetric mode is already saturated at **E*=15 MeV**, at larger E* distribution only becomes wider, minimum at **A/2** is given by competition between interaction & liquid-drop energies.

For 258Fm(sf), potential shows two wide asymmetric minima separated by small local maximum around symmetry. Shell corrections establish position of maxima in yield.

With increasing E*, shell starts to be washed out but remains rather strong for **128Sn+130Sn**.

For 258Fm(n_th,f), at symmetry strong shell fixes minima of PES at small deformations which lead to large [small] interaction potential [liquid-drop energy] compared to neighboring DNS. Damping of shell for asymmetric DNS reduces asymmetric yields, dominant symmetric mode is enhanced due to shell closure of **Sn** nuclei.

At E*=50 MeV, shell effects are completely damped, stiffness of nuclear surface reaches its minimal value, mass yield becomes wider with further increasing E*.

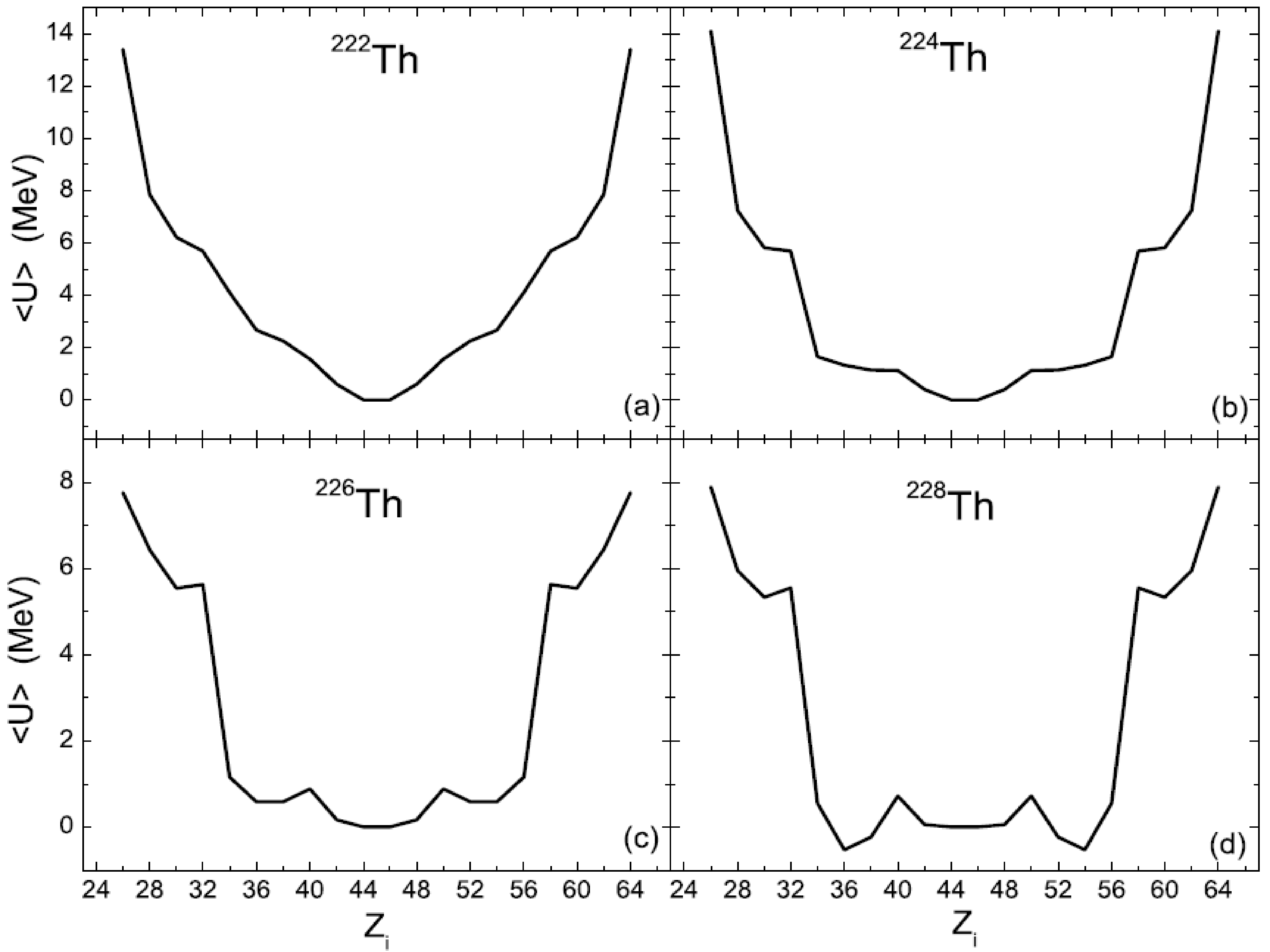

222Th
224Th
226Th
228Th
(a)
(b)
(c)
(d)
<U> (MeV)
<U> (MeV)
Zi
Zi
0
2
4
6
8
10
12
14
24
28
32
36
40
44
48
52
56
60
64

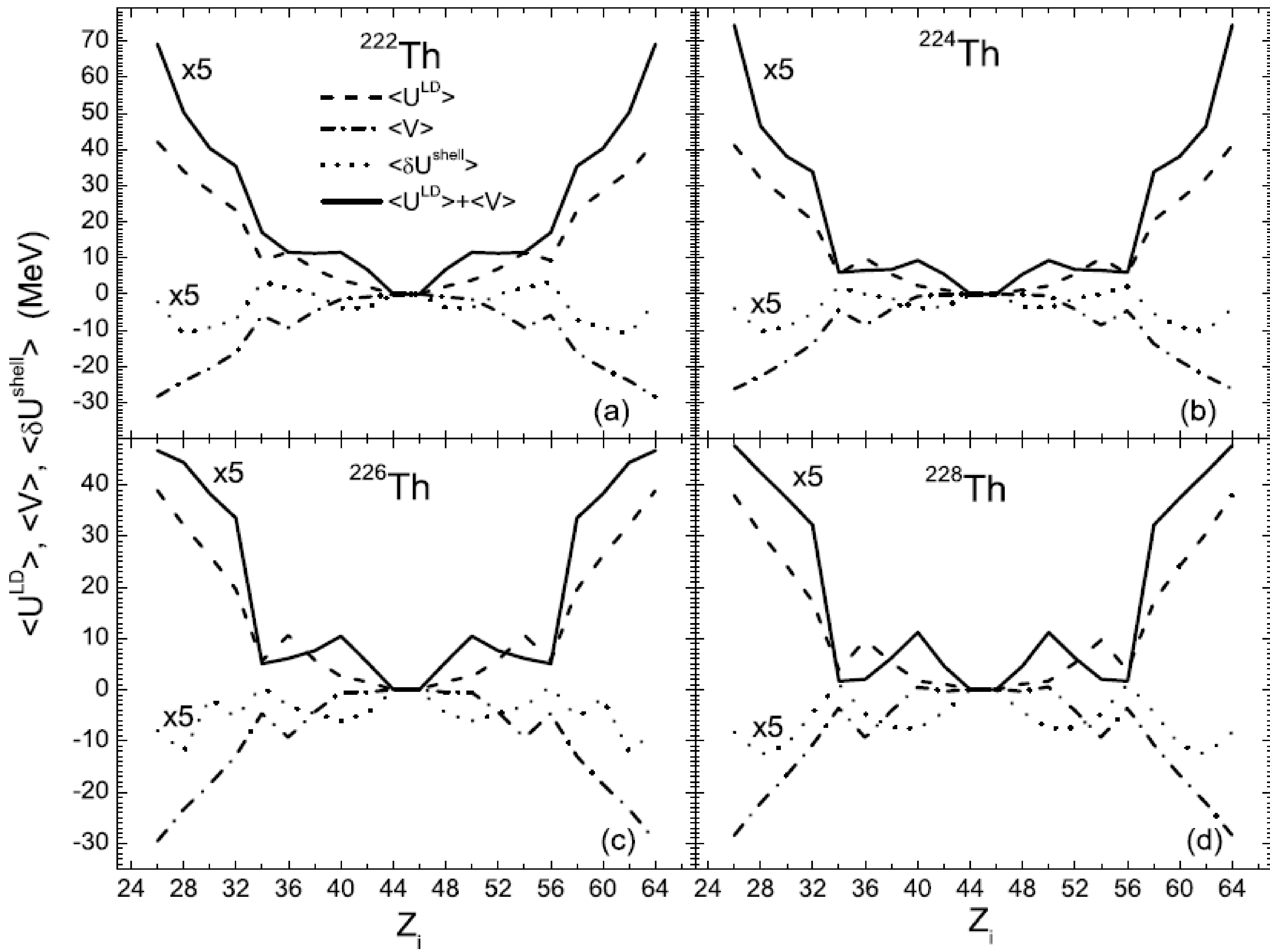

222Th
224Th
226Th
228Th
x5
<ULD>
<V>
<δUshell>
<ULD>+<V>
(a)
(b)
(c)
(d)
<ULD>, <V>, <δUshell> (MeV)
Zi

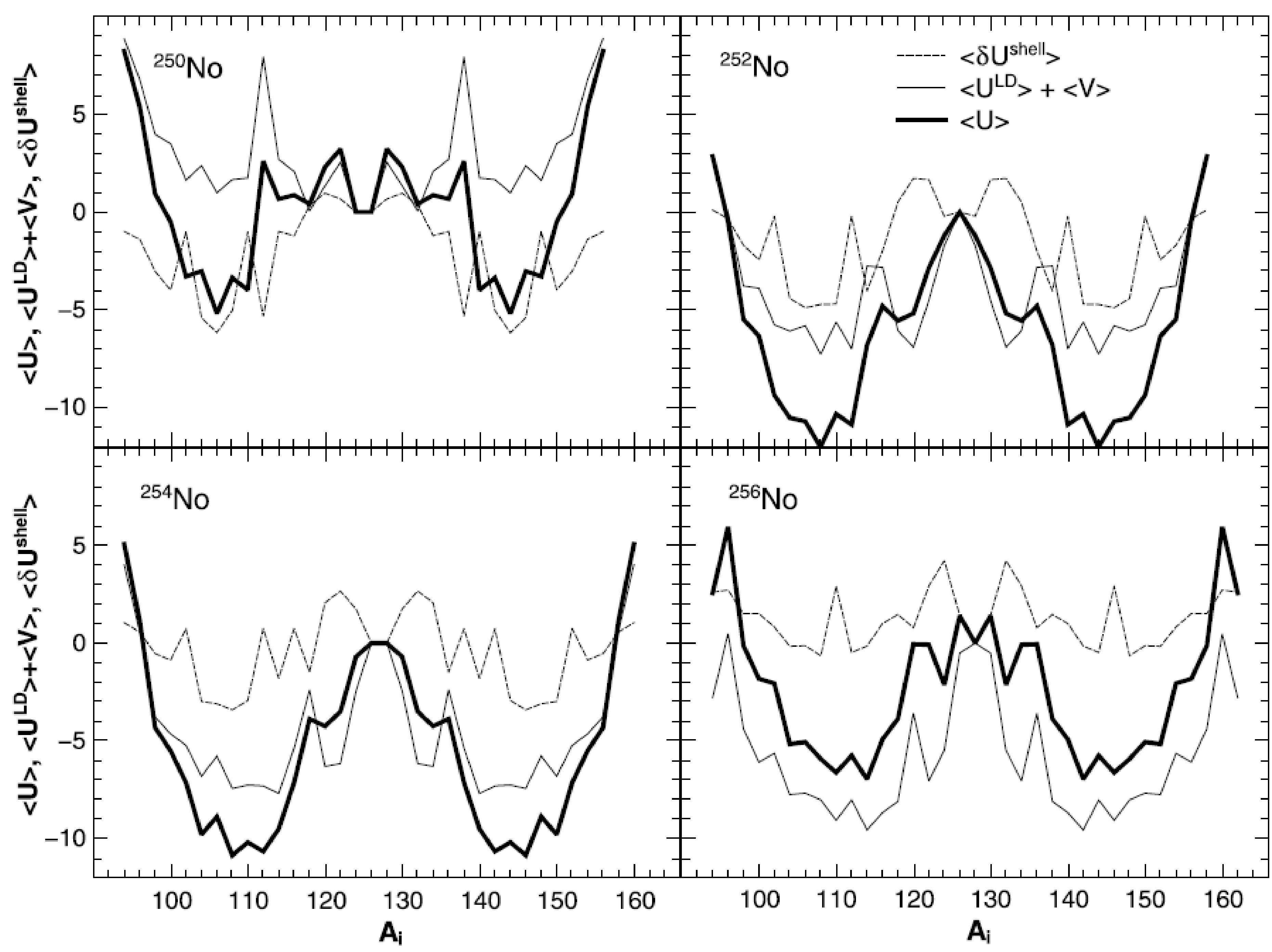

^{250}No
^{252}No
^{254}No
^{256}No
$<\delta U^{shell}>$
$<U^{LD}> + <V>$
$<U>$
$<U>, <U^{LD}>+<V>, <\delta U^{shell}>$
A_i
5
0
−5
−10
100
110
120
130
140
150
160